TABLE 1. Primer Pairs

Name (rat)	Accession number	Primer sequence	Between residues
GluR1/flip	M38060	GAAGCAAGGACTCCGGAAGTAA	2363 and 2384
		GTAGAACACGCCTGCCACATT	2433 and 2413
GluR1/flop	M36418	GTCCGCCCTGAGAAATCCA	2259 and 2277
		AGCCCCTGCTCGTTCAGTT	2315 and 2297
GluR2/flip	M38061	GGAACCCCAGTAAATCTTGCAGT	2720 and 2742
		GAGTCCTTGGCTCCACATTCAC	2826 and 2805
GluR2/flop	M36419	CATCGCCACACCTAAAGGATC	2262 and 2282
		CAATTTGTCCAACAGGCCTTGT	2349 and 2328
GluR3/flip	M38062	GGAATGTGGAGCCAAGGACTC	2391 and 2411
		GCTCAGGCTTAGAGCACTGGTC	2448 and 2427
GluR3/flop	M36420	GGCAACCCCTAAAGGCTCAG	2280 and 2299
		AATACTGCCAGGTTAACAGCATTTC	2330 and 2306
GluR4/flip	M38063	TTTTGAAACTCAGTGAGGCAGG	2315 and 2336
		CGTACCACCATTTGTTTTTCAGC	2371 and 2349
GluR4/flop	M36421	CCTCTTGGACAAATTGAAAAACAA	2337 and 2360
		CCGCTGCCACATTCTCCTT	2393 and 2375

sulphonic acid (HEPES), 5; $CaCl_2$, 1; $MgCl_2$, 4; ethyleneglycol-bis-N,N,N′,N′-tetraacetic acid (EGTA), 5; and N-methyl-D-glucamine (NMDG), 10. The pH of the solution was adjusted to 7.3 with 1 N HCl. The pipette resistance was 5–9 MΩ. The external solution contained (in mM): KCl, 2.5; NaCl, 110; $CaCl_2$, 3; $BaCl_2$, 6; glucose, 15; and HEPES, 5. The pH was adjusted to 7.4 with NMDG. The external KA or drugs were applied rapidly using the Y-tube technique (Min et al., 1996), which allows the complete exchange of the external solution surrounding a cell within 20 ms. The temperature monitored in the recording dishes was 33–34°C. PEPA and cyclothiazide were dissolved in DMSO at 0.1 or 0.3 M, and the solutions were diluted into the control medium to prepare working solutions. The maximal concentration of DMSO in the medium was 0.1%. The electrophysiological data are presented as mean ± SEM in the text and the SEM is indicated by a vertical bar in the figures.

SYBR Green-Based Real-Time Quantitative RT-PCR

Total RNAs were prepared from 2×10^6 microglial cells with RNeasy RNA purification kit (Qiagen, Valencia, CA) according to the manufacturer's protocol. First-strand cDNA synthesized from 1 μg total RNA with random hexamer primers was used as template for each reaction. SYBR Green-based real-time quantitative RT-PCR was performed as described (Aoki et al., 2002). Applied Biosystems 7700 Sequence Detection System (Foster City, CA) was used for the signal detection and the PCR was performed in 1 × SYBR Green Master mix with 500 nM of each primer (Applied Biosystems). For standardization and quantification, rat β-actin or GAPDH was amplified simultaneously. Primer sequences were designed with Primer Express Software (Applied Biosystems). The primer pairs for each GluRs-flip/flop were shown in Table 1.

PCR conditions were 95°C for 10 min, followed by 40 cycles at 95°C for 15 sec and 60°C for 1 min. The threshold cycle of each gene was determined as the PCR cycle at which an increase in fluorescence was observed above the baseline signal in an amplification plot (Wada et al., 2000). The normalized expression level of target (dCt) was calculated as the difference in threshold cycles for target and reference (β-actin or GAPDH). The formula 2^{-dCt} was used to calculate relative expression levels for target molecules compared to the reference. To reduce possible error, RT-PCR reaction was performed three times and averaged 2^{-dCt} values were obtained.

Assay of TNF-α

The isolated microglial cells were seeded in a 96-well plate at a density of 1.5×10^5 cells/ml and stabilized for 30 min. Then the cells were treated with 1 mM Glu or 300 μM KA with or without PEPA, CTZ, or PD 098059, an MAPK inhibitor. To see the effect of Ca^{2+}-free or Na^+-free solution, the following solutions were used (in mM); KCl, 2.5; NaCl, 110; $BaCl_2$, 6; glucose, 15; and HEPES, 5 (Ca^{2+}-free solution); and KCl, 2.5; choline Cl, 110; $CaCl_2$, 3; $BaCl_2$, 6; glucose, 15; and HEPES, 5 (Na^+-free solution). The pH of the solution was adjusted to 7.4 with NMDG. After treatment for 3 h, the amount of rat TNF-α released into the culture medium was measured using an ELISA Kit following the manufacturer's protocol (Biosource, Camarillo, CA). The absorbency at 450 nm was measured with a Microplate Reader (ImmunoMini NJ-2300, Narge Nunc International, Denmark). The data are presented as mean ± SEM of 4–5 experiments.

Immunocytochemistry

Microglial cells cultured on glass coverslips were initially rinsed three times for 5 min per rinse with PBS. Cells were fixed with freshly prepared 4% paraformaldehyde for 30 min at room temperature. Following several rinses with PBS, the cells were permeated with 0.1% Triton-X-100 in PBS for 15 min, then incubated for 60 min in a blocking solution containing 2% bovine

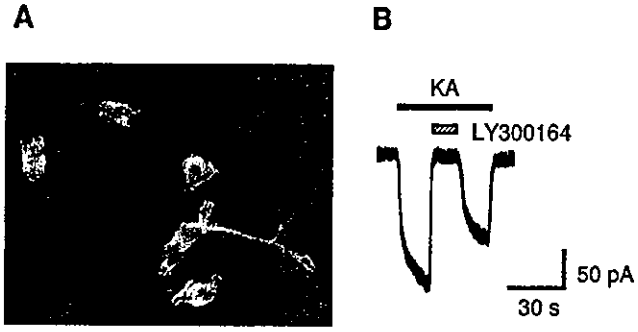

Fig. 1. Identification of microglia and KA-induced current. **A:** Microglial cells were identified using fluorescent probe isolectin-B_4 under the fluorescent microscope combined with phase-contrast modes. Scale bar = 12.5 μm. **B:** Membrane current induced by 300 μM KA was completely blocked by 100 μM LY300164, a selective antagonist of AMPA receptors. The holding potential was −60 mV. Similar results were obtained in four other cells.

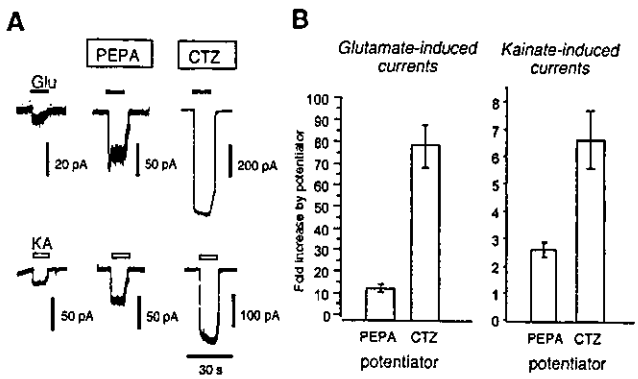

Fig. 2. Potentiating effect of PEPA and CTZ on AMPA receptor in microglial cells. **A:** Effect of PEPA (100 μM) and CTZ (100 μM) on Glu (300 μM)- and KA (300 μM)-induced inward current. The holding potential was −60 mV. All currents were induced in one cell. Similar results were obtained in three other cells. Note the different calibrations. **B:** Effect of each potentiator (100 μM) on Glu (300 μM)- and KA (300 μM)-induced currents recorded at −60 mV. Each bar represents mean ± SEM.

serum albumin (BSA) plus 2% FCS in PBS. Following 3 × rinses with 1% BSA in PBS, the cells were incubated overnight at 4°C with primary antibody diluted in 1% BSA in PBS. The primary antibodies used was rabbit anti–rat TNF-α (1:100; Endogen, MA). Subsequently, cells were rinsed six times for 5 min per rinse, with 1% BSA in PBS and then incubated with Alexa Fluor 594-coupled secondary antibodies (1:500; Molecular Probes, Eugene, OR) for 60 min. Following further wash of six times with 1% BSA in PBS and a final wash with PBS alone, the coverslips were mounted on ethanol-cleaned slides using fluorescence mounting medium (Vector Laboratories, CA) and visualized using a fluorescent microscope system as mentioned above. Images were obtained using a 40× objective with the acquisition setting at 1,300 × 1,030 pixels resolution. Control experiments in which the primary antibody was omitted were performed to determine antibody specificity.

RESULTS

AMPA-Type Glutamate Receptors in Microglia

Most of the isolated cells were microglia (~ 99%) and showed small round- or rod-shaped cell bodies with no or a few thick processes (Fig. 1A). We observed Glu- or KA-induced currents in whole-cell patched microglial cells under voltage-clamp conditions at the holding potential of −60 mV. KA induces a nondesensitizing inward current through AMPA receptors (Patneau and Mayer, 1990). In the previous study, KA induced sustained inward currents in a concentration-dependent manner with half-activation concentration of 330 μM, and the response to 300 μM KA was totally suppressed in the presence of 10 μM CNQX (Noda et al., 2000). In the previous study, it was predicted that KA-induced currents were mainly due to AMPA receptors because of low responsiveness to concanavalin A. In the present study, KA-induced currents were completely blocked by LY300164 (100 μM), a selective antagonist of AMPA receptors (Czuczwar et al., 1998), suggesting that most of the functional glutamate receptors in cultured rat microglia were revealed to be AMPA receptors, but not KA receptors (n = 5; Fig. 1B).

Effect of PEPA and Cyclothiazide on Glutamate- and Kainate-Induced Currents in Microglia

We studied the effect of PEPA and CTZ on Glu- and KA-induced currents in whole-cell patched microglial cells (Fig. 2A). It has been shown that both modulators produced marked potentiation of AMPA-preferring receptor-mediated response (Sekiguchi et al., 1997, 1998; Shen et al., 1999). Each of glutamate receptor agonists (Glu or KA, 300 μM) was first applied to microglial cell, and after 3-min wash, PEPA (100 μM) or CTZ (100 μM) was preloaded for 1 min. Then, each agonist was again applied in the presence of PEPA or CTZ (each solution was applied after 3-min wash). Since we could not observe the fast transient peak of AMPA receptor current, we measured the amplitudes of steady-state component of the Glu responses. Therefore, the potentiating ratios of Glu-induced currents were overestimated compared to those of KA-induced currents. Both PEPA and CTZ clearly potentiated the steady-state level of Glu- and KA-induced currents. However, PEPA was much less potent than CTZ in rat microglia.

The potentiating effects of PEPA and CTZ were summarized in Figure 2B. Figure 2B (left) shows the effect of the modulators on Glu-induced sustained currents. The potentiation by PEPA and CTZ was 15.2 ± 2.0 fold (n = 30) and 79.2 ± 9.7 fold (n = 17), respectively. Similarly, Figure 2B (right) shows the effect on KA-induced currents. The extent of potentiation of KA-induced currents by both modulators was much weaker

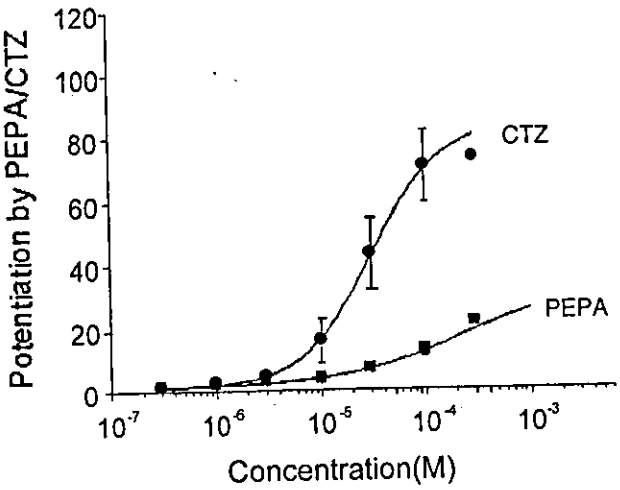

Fig. 3. Dose-dependent potentiation of Glu-induced currents by PEPA and CTZ. The potentiation by PEPA (squares) or by CTZ (circles) was calculated as follows: current amplitude induced by Glu (300 μM) plus PEPA or CTZ/current amplitude induced by Glu (300 μM) alone. The theoretical curves indicate the best fit to the data according to logistic function, $I = I_{max} \times 1/[1 + (EC_{50}/ligand)^n]$. Values are mean ± SEM (n = 4–20).

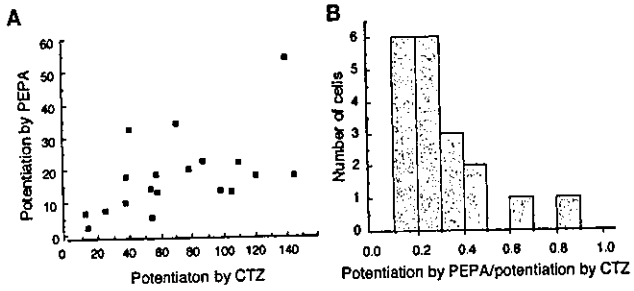

Fig. 4. Distribution of P/C ratio. A: A scatter plot illustrating potentiation by PEPA of Glu-induced inward current versus potentiation by CTZ of Glu-induced inward current in each of the cultured microglial cells tested (n = 19). B: The distribution of P/C ratio among the rat cultured microglia. Abscissa scale shows P/C ratio, which was calculated as follows: potentiation by 100 μM PEPA (as calculated above)/potentiation by 100 μM CTZ (as calculated above). Ordinate scale shows number of cells.

than that of Glu-evoked currents: PEPA 2.7 ± 0.3 fold (n = 11) and CTZ 6.7 ± 1.1 fold (n = 8).

Concentration-Dependent Potentiation of Glu-Induced Currents by PEPA and CTZ

PEPA potentiated Glu-induced currents in a dose-dependent manner (Sekiguchi et al., 1997; Shen et al., 1999). Figure 3 shows the fold increase of Glu (300 μM)-induced currents by PEPA and CTZ with different concentration. Both PEPA (10^{-6} to 10^{-3} M) and CTZ (10^{-6} to 10^{-3} M) potentiated Glu-induced currents in a concentration-dependent manner in rat microglial cells. The EC_{50} for potentiation by PEPA and CTZ were 210 μM (Hill coefficient = 0.79) and 31 μM (Hill coefficient = 1.32), respectively.

Heterogeneity of AMPA Receptor in Microglia

It has been reported that a comparison of the action of PEPA versus CTZ (P/C ratio) facilitates the detection of the splice variant heterogeneity of AMPA receptors in rat hippocampal cultures (Sekiguchi et al., 1998). Xenopus oocytes expressing recombinant AMPA receptors predominantly composed of flip splice variants showed lower P/C ratios (0.19–0.50), while those consisting of flop variants showed higher P/C ratios (1.8–2.2) (Sekiguchi et al., 1998). According to the previous report, we investigated the cell-to-cell variations of flip and flop variants of AMPA receptors in rat microglia. The scatter plots in Figure 4A illustrated the potentiation by PEPA versus potentiation by CTZ of Glu-induced currents in each of the cultured microglial cells (n = 19). The potentiation by PEPA and potentiation by CTZ showed pronounced cell-to-cell variations. The population of Glu-induced currents by PEPA varied between 2.5- and 54-fold, and the potentiation by CTZ varied between 11.3- and 145-fold (Fig. 4A). The histogram in Figure 4B, which was plotted from the data shown in Figure 4A, shows the number of cells included in each range of the P/C ratio. The cultured microglia we used showed cell-to-cell variations with respect to the P/C ratio (0.1–0.9). In contrast to the results in hippocampal neurons (Sekiguchi et al., 1998), most of microglial cells (17/19 cells, 89%) exhibited P/C ratios of lower than 0.5. These results suggest that the heterogeneity of microglial cells may be more restricted than that of hippocampal neurons.

Expression of AMPA Receptor Subunits and Their Splice Variants in Rat Microglia

To prepare the microglial cell culture for RT-PCR study, great care was taken to eliminate the contamination of other cell types so that the purity was more than 99%. Quantitative RT-PCR analysis of AMPA receptors showed that rat primary cultured microglia express substantial amount of flip variants of GluR1–4 and flop variant of GluR2 and GluR4 (Fig. 5). In contrast, flop variant of GluR1 and GluR3 were barely detected. Overall, flip variants of GluRs appear to be expressed dominantly in rat cultured microglia, in accordance with the results that CTZ was a more potent enhancer of AMPA receptors in rat microglia.

Current-Voltage Relationship of Glu-Induced Currents and Effect of PEPA and CTZ

Figure 6 shows the current-voltage (I-V) relationship of the Glu (300 μM)-induced response in the absence or presence of the modulators (100 μM). The microglial cells were voltage-clamped at −60 mV. The I-V rela-

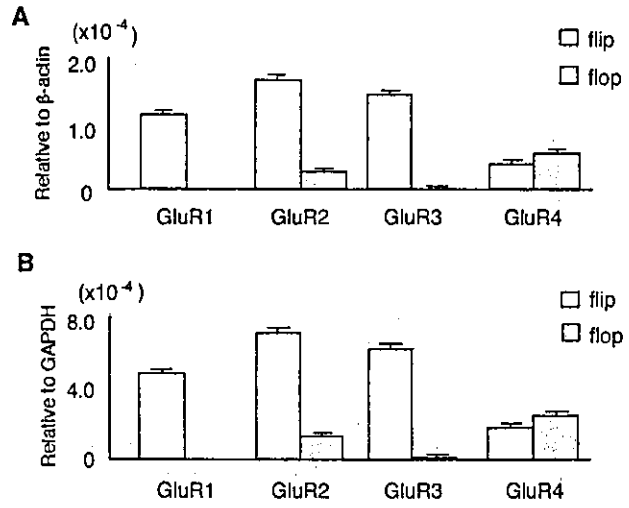

Fig. 5. Quantitative RT-PCR of GluR1–4 and their splice variances (flip/flop). The expression level of each receptor mRNA was normalized to the level of β-actin mRNA (**A**) or GAPDH mRNA (**B**) and was shown as relative values when β-actin or GAPDH mRNA level is 1.

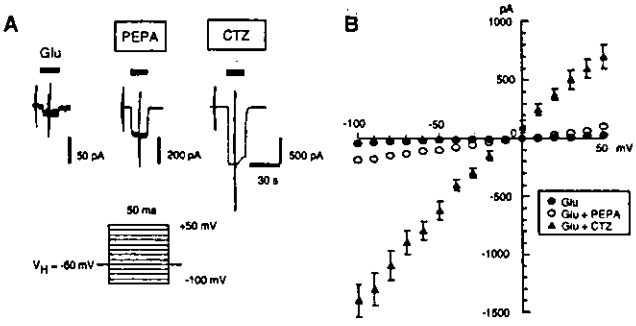

Fig. 6. I-V relationship of Glu-induced currents. **A:** 300 μM Glu-induced currents in the absence and presence of 100 μM PEPA or CTZ were obtained and voltage pulses with 50-ms duration were applied between −100 and 50 mV from the holding potential of −60 mV (shown below) before and during the application of Glu. **B:** The voltage-dependence of Glu-induced currents was obtained by subtracting the currents before application of Glu. Each point represents the mean ± SEM (n = 3).

tionships were obtained at membrane potentials between 50 mV and −100 mV in 10 mV steps with 50-ms duration before and during application of Glu in the absence or presence of modulators. The current amplitude was measured at the end of each pulse (Fig. 6A). Glu-induced I-V was obtained by subtracting the current before application of Glu, which reversed approximately at 0 mV under each condition (Fig. 6B). PEPA and CTZ potentiated the amplitude of AMPA receptor responses with little change in ionic permeability.

Inhibition of Glu- and KA-Activated Release of TNF-α From Microglia by PEPA and CTZ

Microglial cells are known to produce cytokines after cellular activation (McGeer et al., 1993; Meda et al., 1995). When microglial cells were activated with Glu or KA, the production of TNF-α was significantly enhanced (Noda et al., 2000). Accordingly, we predicted that the production of TNF-α would significantly increase when the Glu- or KA-induced currents were significantly enhanced. However, we found that this was not the case in our study. Surprisingly, the production of TNF-α by Glu or KA was rather suppressed in the presence of PEPA or CTZ (Fig. 7A). Similar to our previous report, the production of TNF-α was significantly enhanced by 1 mM Glu or KA after 3-h incubation. However, when PEPA or CTZ at the concentration of 100 μM were added, the production of TNF-α was suppressed, especially with CTZ. The production of TNF-α in the presence of PEPA or CTZ alone was the same as the control (data not shown). Immunostaining of TNF-α using anti-TNF-α-specific antibody showed strong induction of TNF-α by application of 1 μg/ml lipopolysaccharide, which also triggers microglial chemokine and cytokine. The moderate increase in TNF-α was observed by 1 mM Glu. In accordance with the result in Figure 7A, application of Glu together with 100 μM CTZ nullified the induction of TNF-α (Fig. 7B).

To investigate the contribution of excess influx of Na^+ or Ca^{2+} ions to the inhibition of TNF-α release by CTZ, the culture medium was exchanged by Na^+-free or Ca^{2+}-free solution and TNF-α assay was performed the same way. The increase in TNF-α release by Glu or KA was not observed when extracellular Na^+ or Ca^{2+} ions were eliminated (Fig. 8A). Coapplication of CTZ at concentration of 10 or 100 μM did not have significant effect either. In both Na^+-free and Ca^{2+}-free solution, the absolute amounts of control TNF-α release were much higher than those obtained in the culture medium. The reason was not known but it was predicted that Na^+-free or Ca^{2+}-free conditions might be stressful circumstances for microglia and hence microglia was activated to release TNF-α. Even under these circumstances, application of microglial cells with 100 ng/ml LPS caused 5–6 times increase in TNF-α release (data not shown). These results suggest that influx of Na^+ and Ca^{2+}-ions through AMPA receptor is important for Glu-induced increase in TNF-α release.

TNF-α release by Glu or KA may be due to MAPK activation as was reported by corticotropin releasing hormone (Wang et al., 2003). In this case, the inhibitory effects of PEPA and CTZ might be due to the inhibition of MAPK. However, TNF-α release by Glu (not shown) or KA was not affected by preapplication of microglia with 5 μM PD 098059, an MAPK inhibitor, for 24 h (Fig. 8B). Our result suggests that activation of MAPK was not required for the Glu-induced TNF-α release and therefore MAPK inhibitor did not mimic the inhibitory effects of CTZ or PEPA.

DISCUSSION

Although properties of cultured microglia can considerably differ from corresponding cells in situ, the present study confirmed that rat microglia express

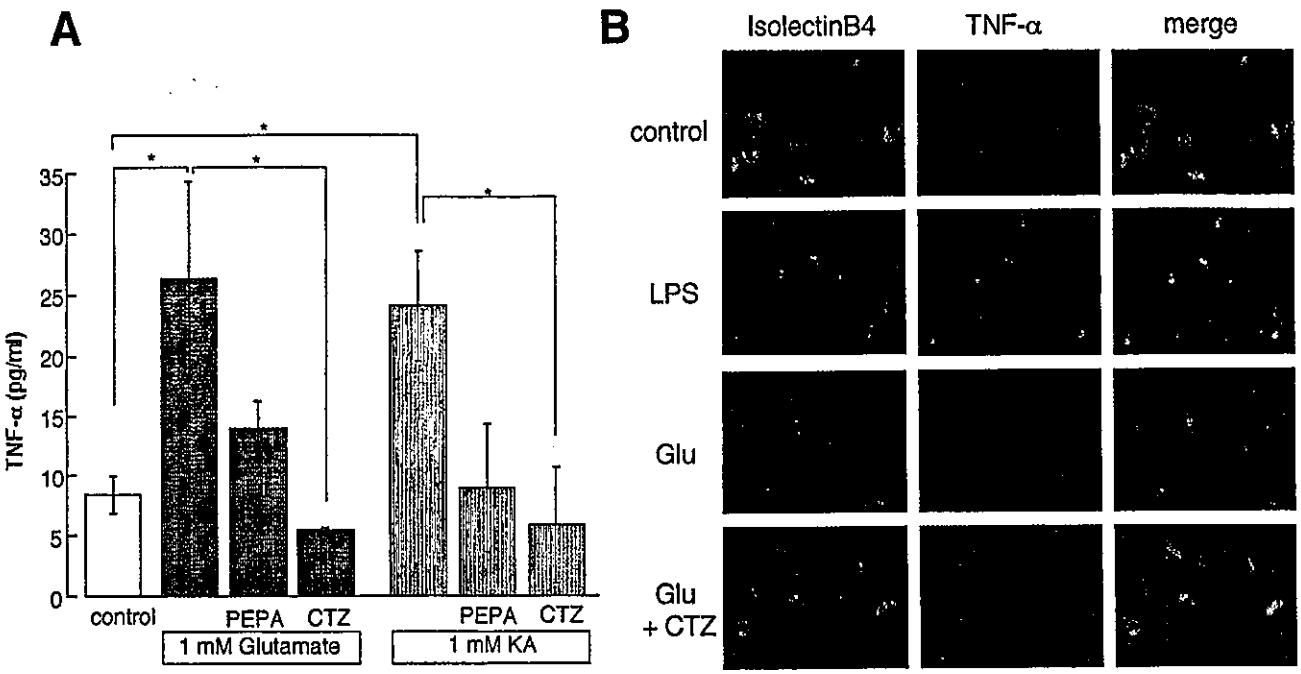

Fig. 7. Effects of PEPA and CTZ on Glu- and KA-induced TNF-α release. **A:** The amount of TNF-α released into the culture medium was measured by ELISA. Production of TNF-α by 1 mM Glu or KA was rather attenuated by addition of PEPA (100 μM) or CTZ (100 μM). Asterisk, $P < 0.05$ compared with control (one-way ANOVA). **B:** Immunofluorescence of TNF-α in microglia treated with 1 μg/ml LPS, 1 mM Glu, or 100 μM CTZ together with 1 mM Glu for 3 h. Microglial cells were double-stained with isolectin-B_4 (FITC-labeled; green) and anti-TNF-α antibody (Alexa Fluor 594-labeled; red).

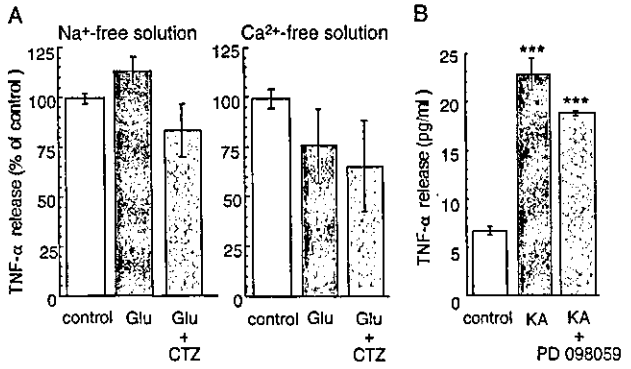

Fig. 8. Effects of Na^+- and Ca^{2+}-free extracellular solution and MAPK inhibitor on TNF-α release. **A:** TNF-α release was not significantly activated by Glu in Na^+-free solution and even cancelled in Ca^{2+}-free solution. Coapplication of CTZ tended to attenuate the TNF-α release further. **B:** Preapplication of microglial cells with an MAPK inhibitor, PD 098059 (5 μM), did not have significant effect on KA-activated TNF-α release. Triple asterisk, $P < 0.001$ compared with control (one-way ANOVA).

AMPA-type Glu receptors and found that little functional KA receptors were expressed by using a new AMPA-selective inhibitor. In a previous report (Noda et al., 2000), RT-PCR study suggested that rat microglia might also express KA-type Glu receptors. Using KA as an agonist of AMPA/KA type of Glu receptor, which gave noninactivating inward currents, we introduced the specific inhibitor of AMPA-type Glu receptors, LY300164, which corresponds to GYKI53773 and a noncompetitive antagonist of AMPA receptor-mediated responses (Czuczwar et al., 1998; Abraham et al., 2000). In our study, the sustained inward current in the presence of 300 μM KA was completely inhibited by 100 μM LY300164 in five cells tested (Fig. 1), as shown in cultured rat spinal cord motoneurons (Van Damme et al., 2002). These results confirmed that KA-induced currents in cultured rat microglia were mostly AMPA receptor-mediated currents and KA receptors were barely functional, though concanavalin-sensitive KA receptors could be recorded in some cells (Noda et al., 2000).

The AMPA receptor-mediated responses either by Glu or KA were greatly enhanced by PEPA and CTZ (Fig. 2), and the effects of PEPA and CTZ were concentration-dependent (Fig. 3). Figure 2B compares the action of PEPA and CTZ on Glu- and KA-evoked currents. Glu responses were smaller than KA responses in the absence of modulators (Fig. 2A; left traces). This is attributable in part to stronger desensitization of responses to glutamate than KA at AMPA receptors (Patneau and Mayer, 1991; Patneau et al., 1993). Since we could not observe fast transient currents with our Y-tube system, all respective quantification was done at the steady-state components, which usually reach less than 10% of the effective amplitudes. Consequently, the overall amplification by PEPA and CTZ appear to be overestimated. Though there was a limitation of measurement system, smaller potentiation by PEPA on both Glu- and KA-induced currents than that by CTZ was observed.

Our results revealed that microglial cells consist of multiple populations with respect to P/C ratio (Fig. 4), which suggests that multiple AMPA receptor subtypes are expressed in the cultured microglia we used. The P/C ratio varies with subunit and splice variant compositions. Our investigation in microglia gave relatively low P/C ratio (0.1–0.9) with most abundant distribution between 0.1 and 0.5 (89%). The low P/C ratio results from a combination of the weak potentiation by PEPA and potent action by CTZ. Since CTZ and PEPA act preferentially on flip and flop variants, respectively, cells exhibiting a low P/C ratio (< 0.5) are supposed to express flip variants predominantly. In the cultured hippocampal cells, two populations exhibited characteristic P/C ratio: low P/C ratio (0–0.15, 34%) and high P/C ratio (> 2.00, 1%) with intermediate P/C ratio (0.25–1.20, 65%) (Sekiguchi et al., 1998). Taken together, the distribution of different combination of flip/flop variants were more restricted in microglia than hippocampal cells.

Our electrophysiological observation that rat microglia may express flip variants preferentially was further confirmed by quantitative RT-PCR (Fig. 5). The P/C ratio of 0.1–0.5 in the majority of the cultured microglia is likely explained by the predominant expression of flip forms as shown in oocytes expressing GluR1-3 (Sekiguchi et al., 1998). In addition, GluR4 variants may contribute to not only heterogeneity but also activation of microglia (Mennini et al., 2002).

We previously reported that rat microglia express GluR2 and showed low Ca^{2+} permeability with or without CTZ (Noda et al., 2000). It is well known that AMPA receptor lacking GluR2 (RNA-edited form) conduct calcium ions (Hollmann et al., 1991; Hume et al., 1991; Burnashev et al., 1992). In the present study, we applied series of short pulses to obtain quick I-V relationships instead of changing the holding potential. The I-V relationships of Glu-induced currents in rat microglia were quite similar to those we obtained before and were quite linear in the presence of PEPA as well. It confirms that both PEPA and CTZ do not affect rectification or ion permeability of AMPA receptors (Fig. 6).

Activation of microglia is often observed in pathological conditions. Regulation of microglial reactivity has been proposed to be a key factor for neuroprotection in brain disorders, including neurodegenerative diseases (Streit and Kincaid-Colton, 1995; Wyss-Coray et al., 2001; Polazzi and Contestabile, 2002). Though the physiological role of AMPA receptor in microglia still remains unclear, the enhancement of AMPA receptor in microglia may have a possibility to contribute to neuroprotection. Actually, PEPA ameliorates postischemic memory impairment even with ischemia-induced structural damage to the brain (Sekiguchi et al., 2001). In the present study, we unexpectedly observed that coapplication of PEPA with Glu attenuated the TNF-α release stimulated by Glu or KA alone in microglia. More surprisingly, coapplication of CTZ with Glu or KA almost completely nullified the increase in TNF-α release (Fig. 7A). It means that augmentation of AMPA-induced currents has negative feedback control on the release of TNF-α, though the mechanism is not known yet. The inhibition rate of TNF-α release was not significantly different between 10 and 100 μM of PEPA or CTZ (not shown), suggesting the concentration dependence of PEPA and CTZ on TNF-α release might be different from that on current augmentation.

The mechanism of Glu- or KA-activated TNF-α release was still unknown. However, the new aspects that extracellular Na^+ and Ca^{2+} ions are required for Glu- or KA-induced TNF-α release were obtained (Fig. 8A). It was reported that Na^+ entry through AMPA receptors results in voltage-gated K^+ channel blockade in glial cells (Borges and Kettenmann, 1995; Schröder et al., 2002). Since voltage-dependent K^+ currents in microglia were small in our experimental condition and it was reported that resting microglia did not have outward K^+ currents (Kettenmann et al., 1993), it was hard to distinguish whether potentiation of AMPA receptor caused the inhibition of voltage-dependent K^+ channel or not. Apart from the effects on K^+ channels, it may be predicted that excess influx of Na^+ ions could cause inhibitory effects on subsequent function in microglia with unknown mechanism. Indeed. elimination of Na^+ not only prevented the effects of PEPA and CTZ but also Glu- or KA-activated TNF-α release itself. Elimination of extracellular Ca^{2+} ions had more clear effect on the inhibition of Glu-activated TNF-α release, as was predicted by the report that intracellular Ca^{2+} ions were important in TNF-α production (Fig. 8A, right) (Combs et al., 1999). We further investigated whether PEPA or CTZ had inhibitory effects on TNF-α release by other stimulant, for example, lipopolysaccharide (LPS). However, there was no significant inhibition by PEPA or CTZ, even in the presence of Glu (data not shown). Therefore, the inhibitory effect of PEPA and CTZ was not a nonspecific effect on general production of TNF-α, and the inhibitory effect due to the augmentation of AMPA receptor could not compete with LPS-activated TNF-α.

Another question was whether Glu-activated TNF-α release was MAPK-dependent or not. Because it was reported that LPS-induced TNF-α release was augmented by p38 MAPK (Lee et al., 2000), the effect of PEPA or CTZ could be due to the modulation of MAPK activity. However, application of one of the MAPK-inhibitor, PD 098059, to microglial cells did not significantly affect Glu-activated TNF-α release. Immunoreactivity of phospho-p38 MAPK also showed no difference between the control, Glu-treated, and Glu with CTZ-treated rat cultured microglia (data not shown). These results indicate that the Glu-induced TNF-α release and their modulation by CTZ were independent on MAPK activity.

The contribution of metabotropic Glu receptors (mGluRs) to the formation of TNF-α could also be plausible. Though Glu- and KA-induced TNF-α release was significantly inhibited by CNQX (Noda et al., 2000), expression of mGluRs in microglia was already re-

ported (Biber et al., 1999; Taylor et al., 2002, 2003; Venero et al., 2002). In addition, reduction of TNF-α as well as K^+ currents and NO synthesis was shown in microglia after activation of purinergic receptors (Boucsein et al., 2003).

It is interesting that microglia survived in the presence of CTZ even after 3-h incubation together with Glu (not shown). Low Ca^{2+} permeability of the AMPA receptors may contribute to the survival of microglia. CTZ was reported to cause neuronal and astrocytic cell death due to an excess Ca^{2+} influx into the cells (Brorson et al., 1995; David et al., 1996; John et al., 1999). In contrast to CTZ, PEPA was reported to ameliorate postischemic memory impairment in rats (Sekiguchi et al., 2001). The ameliorating effect of PEPA may not simply be explained by milder blocking of the desensitization of AMPA receptors in neurons. Therefore, we expected that analyzing the effects of PEPA and CTZ on AMPA receptors in microglia might help us understand the effect of these modulators. In addition to the effect on TNF-α, it will be worth trying to investigate how PEPA and CTZ affect the release of other cytokines and growth factors from microglia.

As a conclusion, allosteric modulators of flip and flop type of AMPA receptors are useful tools for detecting the heterogeneity of microglia. Besides, these modulators had inhibitory effect on Glu- or KA-activated TNF-α, though the mechanism was not yet known. Since microglia amplify the release of TNF-α from astrocyte, which was shown in cocultures of astocyte-microglia (Bezzi et al., 2001), and has important role in neuron-glial communication (Fields and Stevens-Graham, 2002), further studies on the effects of modulators in glia-glia or neuron-glia interaction will help us understand the functional role of AMPA receptors in microglia and the difference between CTZ and PEPA in their ameliorating effect in ischemic brain.

ACKNOWLEDGMENTS

The authors thank Dr. T. Harada for his help in their initial experiments, Dr. H. Nakanishi (Kyushu University) for valuable suggestions on the preparation of the primary cultured microglia, Professor N. Akaike (Kyushu University) for providing some of the equipments, and Professor D.A. Brown (University College, London) for reading the manuscript.

REFERENCES

Abraham G, Solyom S, Csuzdi E, Berzsenyi P, Ling I, Tarnawa I, Hamori T, Pallagi I, Horvath K, Andrasi F, Kapus G, Harsing LG Jr, Kiraly I, Patthy M, Horvath G. 2000. New non competitive AMPA antagonists. Bioorg Med Chem 8:2127–2143.

Aoki K, Sun YJ, Aoki S, Wada K, Wada E. 2002. Cloning, expression, and mapping of a gene that is upregulated in adipose tissue of mice deficient in bombesin receptor subtype-3. Biochem Biophys Res Commun 290:1282–1288.

Bezzi P, Domercq M, Brambilla L, Galli R, Schols D, De Clercq E, Vescovi A, Bagetta G, Kollias G, Meldolesi J, Volterra A. 2001. CXCR4-activated astrocyte glutamate release via TNF-alpha: amplification by microglia triggers neurotoxicity. Nat Neurosci 4:702–710.

Biber K, Laurie DJ, Berthele A, Sommer B, Tolle TR, Gebicke-Harter PJ, van Calker D, Boddeke HW. 1999. Expression and signaling of group I metabotropic glutamate receptors in astrocytes and microglia. J Neurochem 72:1671–1680.

Borges K, Kettenmann H. 1995. Blockade of K^+ channels induced by AMPA/kainate receptor activation in mouse oligodendrocyte precursor cells is mediated by Na^+ entry. J Neurosci Res 42:579–593.

Boucsein C, Zacharias R, Farber K, Pavlovic S, Hanisch UK, Kettenmann H. 2003. Purinergic receptors on microglial cells: functional expression in acute brain slices and modulation of microglial activation in vitro. Eur J Neurosci 17:2267–2276.

Brorson JR, Manzolillo PA, Gibbons SJ, Miller RJ. 1995. AMPA receptor desensitization predicts the selective vulnerability of cerebellar Purkinje cells to excitotoxicity. J Neurosci 15:4515–4524.

Burnashev N, Monyer PH, Seeburg B, Sackmann B. 1992. Diavalent ion permeability of AMPA receptor channels is dominated by edited of a single subunit. Neuron 8:189–198.

Combs CK, Johnson DE, Cannady SB, Lehman TM, Landreth GE. 1999. Identification of microglial signal transduction pathways mediating a neurotoxic response to amyloidogenic fragments of β-amyloid and prion proteins. J Neusosci 19:928–939.

Czuczwar SJ, Swiader M, Kuzniar H, Kleinrok Z. 1998. LY300164, a novel antagonist of AMPA/kainite receptors, potentiates the anticonvulsive activity of antiepileptic drugs. Eur J Pharmacol 359: 103–109.

David JC, Yamada KA, Bagwe MR, Goldberg MP. 1996. AMPA receptor activation is rapidly toxic to cortical astrocytes when desensitization is blocked. J Neurosci 16:200–209.

Fields RD, Stevens-Graham B. 2002. New insights into neuron-glia communication. Science 298:556–562.

Hollmann M, O'Shea-Greenfield A, Rogers SW, Heinemann S. 1989. Cloning by functional expression of a member of the glutamate receptor family. Nature 342:643–648.

Hollmann M, Hartley S, Heinemann S. 1991. Ca^{2+} permeability of KA-AMPA-gated glutamate receptor channels depends on subunit composition. Science 252:851–853.

Hume RI, Dingledine R, Heinemann SF. 1991. Identification of a site in glutamate receptor subunits that controls calcium permeability. Science 253:1028–1031.

John CA, Beart PM, Giardina SF, Pascoe CJ, Cheung NS. 1999. Cyclothiazide and GYKI 52466 modulate AMPA receptor-mediated apoptosis in cortical neuronal cultures. Neurosci Lett 268:9–12.

Keinanen K, Wisden W, Sommer B, Werner P, Herb A, Verdoorn TA, Sakmann B, Seeburg PH. 1990. A family of AMPA-selective glutamate receptors. Science 249:556–560.

Kessler M, Rogers G, Arai A. 2000. The norbornenyl moiety of cyclothiazide determines the preference for flip-flop variants of AMPA receptor subunits. Neurosci Lett 287:161–165.

Kettenmann H, Banati R, Walz W. 1993. Electrophysiological behavior of microglia. Glia 7:93–101.

Kreutzberg GW. 1996. Microglia: a sensor for pathological events in the CNS. Trends Neurosci 19:312–318.

Lee YB, Schrader JW, Kim SU. 2000. p38 map kinase regulates TNF-alpha production in human astrocytes and microglia by multiple mechanisms. Cytokine 12:874–880.

McGeer PL, Kawamata T, Walker DG, Akiyama H, Tooyama I, McGeer EG. 1993. Microglia in degenerative neurological disease. Glia 7:84–92.

Meda L, Cassatella MA, Szendrei GI, Otvos L Jr, Baron P, Villalba M, Ferrari D, Rossi F. 1995. Activation of microglial cells by beta-amyloid protein and interferon-gamma. Nature 374:647–650.

Mennini T, Bigini P, Ravizza T, Vezzani A, Calvaresi N, Tortarolo M, Bendotti C. 2002. Expression of glutamate receptor subtypes in the spinal cord of control and mnd mice, a model of motor neuron disorder. J Neurosci Res 70:553–560.

Min BI, Kim CJ, Rhee JS, Akaike N. 1996. Modulation of glycine-induced chloride current in acutely dissociated rat periaqueductal gray neurons by μ-opioid agonist DAGO. Brain Res 734:72–78.

Mosbacher J, Schoepfer R, Monyer H, Burnashev N, Seeburg PH, Ruppersberg JP. 1994. A molecular determinant for submillisecond desensitization in glutamate receptors. Science 266:1059–1062.

Noda M, Nakanishi H, Akaike N. 1999. Glutamate release from microglia via glutamate transporter is enhanced by amyloid-β peptide. Neuroscience 92:1465–1474.

Noda M, Nakanishi H, Nabekura J, Akaike N. 2000. AMPA-kainate subtypes of glutamate receptor in rat cerebral microglia. J Neurosci 20:251–258.

Partin KM, Patenau DK, Mayer ML. 1994. Cyclothiazide differentially modulates desensitization of AMPA receptor splice variants. Mol Pharmacol 46:129–138.

Partin KM, Fleck MW, Mayer ML. 1996. AMPA receptor flip/flop mutants affecting deactivation, desensitization, and modulation by cyclothiazide, aniracetam, and thiocyanate. J Neurosci 16:6634–6647.

Patneau DK, Mayer ML. 1990. Structure-activity relationships for amino acid transmitter candidates acting at N-methyl-D-aspartate and quisqualate receptors. J Neurosci 10:2385–2399.

Patneau DK, Mayer ML. 1991. Kinetic analysis of interactions between kainate and AMPA: evidence for activation of a single receptor in mouse hippocampal neurons. Neuron 6:785–798.

Patneau DK, Vyklicky L Jr, Mayer ML. 1993. Hippocampal neurons exibit cyclothiazide-sensitive rapidly desensitizing responses to kainite. J Neurosci 13:3496–3509.

Polazzi E, Contestabile A. 2002. Reciprocal interactions between microglia and neurons: from survival to neuropathology. Rev Neurosci 13:221–242.

Schröder W, Seifert G, Huttmann K, Hinterkeuser S, Steinhauser C. 2002. AMPA receptor-mediated modulation of inward rectifier K^+ channels in astrocytes of mouse hippocampus. Mol Cell Neurosci 19:447–458.

Sekiguchi M, Mark WF, Mark LM, Takeo J, Chiba Y, Yamashita S, Wada K. 1997. A novel allosteric potentiator of AMPA receptors: 4-[2-(phenylsulfonylamino)ethylthio]-2,6-difluoro-phenoxyacetamide. J Neurosci 17:5760–5771.

Sekiguchi M, Takeo J, Harada T, Morimoto T, Kudo Y, Yamashita S, Kohsaka S, Wada K. 1998. Pharmacological detection of AMPA receptor heterogeneity by use of two allosteric potentiators in rat hippocampal cultures. Br J Pharmacol 123:1294–1303.

Sekiguchi M, Yamada K, Jin J, Hachitanda M, Murata Y, Namura S, Kamichi S, Kimura I, Wada K. 2001. The AMPA receptor allosteric potentiator PEPA ameliorates post-ischemic memory impairment. Neuroreport 12:2947–2950.

Sekiguchi M, Nishikawa K, Aoki S, Wada K. 2002. A desensitization-selective potentiator of AMPA-type glutamate receptors. Br J Pharmacol 136:1033–1041.

Shen Y, Lu T, Yang X-L. 1999. Modulation of desensitization at glutamate receptors in isolated crucian carp horizontal cells by concanavalin A, cyclothiazide, aniracetam and PEPA. Neuroscience 89:979–990.

Sommer B, Keinanen K, Verdoorn TA, Wisden W, Burnashev N, Herb A, Kohler M, Takagi T, Sakmann B, Seeburg PH. 1990. Flip and flop: a cell-specific functional switch in glutamate operated channels of the CNS. Science 249:1580–1585.

Streit WJ, Kincaid-Colton CA. 1995. The brain's immune system. Sci Am 273:54–61.

Sun Y, Olson R, Horning M, Armstrong N, Mayer M, Gouaux E. 2002. Mechanism of glutamate receptor desensitization. Nature 417:245–253.

Taylor DL, Diemel LT, Cuzner ML, Pocock JM. 2002. Activation of group II metabotropic glutamate receptors underlies microglial reactivity and neurotoxicity following stimulation with chromogranin A, a peptide up-regulated in Alzheimer's disease. J Neurochem 82:1179–1191.

Taylor DL, Diemel LT, Pocock JM. 2003. Activation of microglial group III metabotropic glutamate receptors protects neurons against microglial neurotoxicity. J Neurosci 23:2150–2160.

Van Damme P, Van Den Bosch L, Van Houtte E, Eggermont J, Callewaert G, Robberecht W. 2002. Na(+) entry through AMPA receptors results in voltage-gated K(+) channel blockade in cultured rat spinal cord motoneurons. J Neurophysiol 88:965–972.

Venero JL, Santiago M, Tomas-Camardiel M, Matarredona ER, Cano J, Machado A. 2002. DCG-IV but not other group-II metabotropic receptor agonists induces microglial BDNF mRNA expression in the rat striatum. Correlation with neuronal injury. Neuroscience 113: 857–869.

Wada R, Tifft CJ, Proia RL. 2000. Microglial activation precedes acute neurodegeneration in Sandhoff disease and is suppressed by bone marrow transplantation. Proc Natl Acad Sci USA 97:10954–10959.

Wang W, Ji P, Dow KE. 2003. Corticotropin-releasing hormone induces proliferation and TNF-alpha release in cultured rat microglia via MAP kinase signalling pathways. J Neurochem 84:189–195.

Wyss-Coray T, Lin C, Yan F, Yu GQ, Rohde M, McConlogue L, Masliah E, Mucke L. 2001. TGF-beta1 promotes microglial amyloid-beta clearance and reduces plaque burden in transgenic mice. Nat Med 7:612–618.

Available online at www.sciencedirect.com
SCIENCE DIRECT
Molecular Brain Research 126 (2004) 88–97
MOLECULAR BRAIN RESEARCH
www.elsevier.com/locate/molbrainres

Short communication

Microarray expression analysis of gad mice implicates involvement of Parkinson's disease associated UCH-L1 in multiple metabolic pathways

M. Bonin[a], S. Poths[a], H. Osaka[b], Y.-L. Wang[b], K. Wada[b], O. Riess[a,*]

[a] *Department of Medical Genetics, University of Tübingen, Calwerstrasse 7, 72076 Tübingen, Germany*
[b] *Department of Degenerative Neurological Diseases, National Institute of Neuroscience, NCNP, 4-1-1 Ogawahigashi, Kodaira, Tokyo 187-8502, Japan*

Accepted 9 March 2004

Abstract

Parkinson's disease (PD) is thought to be caused by environmental and genetic factors. Mutations in four genes, *α-synuclein*, *parkin*, *DJ-1*, and *UCH-L1*, have been identified in autosomal inherited forms of PD. The pathogenetic cause for the loss of neuronal cells in PD patients, however, remains to be determined. Due to the rarity of mutations in humans with PD, the analysis of animal models might help to further gain insights into the pathogenesis of familial PD. For UCH-L1, deficiency has been described in gad mice leading to axonal degeneration and formation of spheroid bodies in nerve terminals. Here, we investigated the gene expression pattern of the brain of 3-month-old Uch-l1-deficient gracile axonal dystrophy (*gad*) mice by microarray analysis. A total of 146 genes were differentially regulated by at least a 1.4-fold change with 103 being up-regulated and 43 being down-regulated compared with age and sex matched wildtype littermate mice. The gene products with altered expression are involved in protein degradation, cell cycle, vesicle transport, cellular structure, signal transduction, and transcription regulation. Most of the genes were modestly regulated, which is in agreement that severe alteration of these pathways might be lethal. Among the genes most significantly down-regulated is the brain-derived neurotrophic factor which might be one aspect of the pathogenesis in gad mice. Interestingly, several subunits of the transcription factor CCAAT/enhancer binding protein are up-regulated, which plays a central role in most altered pathways.

Theme: Disorders of the nervous system
Topic: Genetic models

Keywords: Ubiquitin; UCH-L1; Parkinson's disease; α-Synuclein; Protein degradation; Microarray chip analysis; Expression

1. Introduction

Parkinson's disease (PD) is the second most common neurodegenerative disorder in humans afflicting 1–2% of the population over 60 [6]. The leading clinical symptoms are mainly caused by loss of dopaminergic neurons of the SN. The cause of the neuronal cell death is not known yet but it is thought that genetic factors might be involved in a significant portion of the patients. In agreement with this assertion, increased concordance rates for PD were found in monozygotic twins (75%) vs. dizygotic twins (22%) [35]. Furthermore, numerous families with autosomal dominant inheritance of PD have been described [10,31,43]. Subsequently, mutations in the *α-synuclein* gene causing a rare autosomal dominant form of PD [18,36] have been described.

α-Synuclein is degraded by the ubiquitin–proteasome pathway [2,40]. Ubiquitin, a highly conserved 76 amino acid protein, is ligated through its C-terminus to the lysine side chains of proteins targeted for degradation by the 26S proteasome [4]. This process is catalyzed by a series of enzymes, called E1, E2, and E3. Mutations in one of the several hundreds of E3 ubiquitin ligases, which has been named parkin, cause an autosomal recessive form of early onset PD [17,26]. Parkin serves also as an E3 ligase [38] for a protein that interacts with α-synuclein and has been designated synphilin 1 [3]. Subsequently, we identified a mutation in synphilin-1 in PD patients [28]. An altered ubiquitin–proteasomal protein degradation pathway might therefore be

* Corresponding author. Tel.: +49-7071-29-76458; fax: +49-7071-29-5171.
E-mail address: olaf.riess@med.uni-tuebingen.de (O. Riess).

0169-328X/$ - see front matter © 2004 Elsevier B.V. All rights reserved.
doi:10.1016/j.molbrainres.2004.03.025

a key event in the pathogenesis of PD [19]. Efficient targeting for degradation by the 26S proteasome requires polyubiquitination. In addition to the isopeptide linkages made to lysines, the ubiquitin C-terminus can also form peptide bonds to α-linked polyubiquitin or ubiquitin followed by a C-terminal peptide extension [34]. This step is catalyzed by a family of Ubiquitin C-terminal hydrolases which are tissue-specific and likely to target distinct substrates. Of these, UCH-L1 is highly expressed in the brain [5,41] and has recently been implicated in PD by the identification of a missense mutation in autosomal dominant PD with reduced penetrance [20]. This I93M mutation was shown to decrease the hydrolytic activity in vitro significantly [20,32]. Although other genetic studies did not find the I93M mutation in further families, a S18Y polymorphism in UCH-L1 was found to be linked to a decreased susceptibility to PD [27,42]. Subsequently, Peter Lansbury's group has shown that the UCH-L1 gene encodes two opposing enzymatic activities indicating that UCH-L1 has an ubiquitin–ubiquitin ligase activity [23]. Inhibitors of the proteasomal pathway in cultured neurons by ubiquitin aldehyde which is a UCH inhibitor cause the formation of protein aggregates and cell death [30]. Most interestingly, UCH-L1 is also part of the Lewy bodies [25].

Although evidence for an altered ubiquitin–proteasomal protein degradation pathway as the cause of PD is striking, the cause of the selective degeneration of dopaminergic neurons in PD patients has not been elucidated. We thought to gain insight into the complex metabolic pattern of neurons by investigating UCH-L1-deficient gracile axonal dystrophy (*gad*) mice using microarray expression analyses. The *gad* mouse is an autosomal recessive spontaneous neurological mutant that was identified in 1984 [37]. Our positional cloning approach successfully identified that the gad mutation is caused by an intragenic deletion of the *Uch-l1* gene including exons 7 and 8 [37]. Subsequent studies have shown that the mutant lacks the expression of UCH-L1 protein [33,37]. Pathologically, the *gad* mouse displays dying-back type of axonal degeneration of the gracile tract. Most interestingly, *gad* mice develop accumulation of amyloid precursor protein (APP) in form of ubiquitin-positive deposits along the sensory and motor nervous systems staining [13], another indication that the gad mutation affects protein turnover. Therefore, direct involvement of an altered ubiquitin system in neurodegeneration has been indicated by this model.

2. Methods

2.1. Mice

Three-month-old male homozygous Uch-l1 deficient (*gad*) mice and their age and sex matched wildtype littermate mice (CBA/RFM) were analyzed in the microarray analysis. Mice were maintained and propagated at National Institute of Neuroscience, National Center of Neurology and Psychiatry (Japan). Experiments using these mice were approved by the Animal Investigation Committee of the Institute.

2.2. Brain tissue preparation and RNA analysis

Mice were killed by cervical dislocation, brains were quickly removed, immersed briefly in ice-cold saline, and whole brains were frozen on dry ice and stored at −80 °C. Total RNA was extracted from mouse whole brain including olfactory bulb, cerebellum and brain stem by using RNeasy kits (Qiagen). The RNA quality was controlled by Lab-on-Chip-System Bioanalyser 2100 (Agilent).

2.3. Microarray analysis

Double-stranded cDNA was synthesized from the total RNA of one whole brain using a Superscript choice kit (Invitrogen) with a T7-(dT)24 primer incorporating a T7 RNA polymerase promoter (Metabion). cRNA was prepared and biotin labeled by in vitro transcription (Enzo Biochemical). Labeled RNA was fragmented by incubation at 94 °C for 35 min in the presence of 40 mM Tris-OAc (pH 8.1), 100 mM KOAc, and 30 mM MgOAc. Labeled, fragmented cRNA (15 μg) was hybridized for 16 h at 45 °C to a MG-U74A mouse genome array (Affymetrix). After hybridization, gene chips were automatically washed and stained with streptavidin–phycoerythrin using a fluidics station. The probe arrays were scanned at 3-μm resolution using a Genechip System confocal scanner made for Affymetrix by Agilent.

Affymetrix Microarray Suite software (version 5.0), MicroDB and Data Mining Tool were used to scan and analyze the relative abundance of each gene based on the intensity of the signal from each probe set. Analysis parameters used by the software were set to values corresponding to moderate stringency (statistical difference threshold = 30, statistical ratio threshold = 1.5). Output from the microarray analysis was merged with the Unigene or GenBank descriptor and saved as an Excel data spreadsheet.

Each cRNA generated from a brain was hybridized on one microarray separately. We ran three arrays analyzing three gad mice vs. two controls allowing a total of six comparisons (3 × 2 matrix). For each comparison, the analysis using the Affymetrix software generates a "difference call" of no change, marginal increase/decrease, or increase/decrease, respectively. Only those genes which were found in at least six of six comparisons similarly adjusted were defined as stringent differentially expressed genes. Genes which were found in five of six comparisons similarly adjusted were defined as moderate differentially expressed genes. The magnitude and direction of expression changes were estimated as Signal Log Ratio (SLR). The log scale used is base 2, making it intuitive to interpret the Signal Log Ratios in terms of multiples of two. Thus, an SLR of 1.0 indicates an increase of the transcript level by two-fold and −1.0 indicates a two-fold decrease. An SLR

Table 1a
List of stringent differentially regulated genes

GenBank ID	slr—Average	slr—S.D.	Gene-information
RNA-metabolism (3)			
AA791742	1.09	0.28	ARP2 actin-related protein 2 homolog (yeast)
AA690583	0.87	0.34	splicing factor proline/glutamine rich (polypyrimidine tract binding protein associated)
AI843586	0.72	0.21	splicing factor, arginine/serine rich 9 (25 kDa)
Vesicle-transport-proteins (3)			
U60150	0.8	0.24	vesicle-associated membrane protein 2
AB025218	0.71	0.11	coated vesicle membrane protein
D12713	0.68	0.15	SEC23A (*S. cerevisiae*)
Cellular structure proteins (4)			
AF067180	1	0.16	kinesin family member 5C
AB023656	0.6	0.21	kinesin heavy chain member 1B
M21041	0.73	0.21	microtubule-associated protein 2
M18775	−0.69	0.22	microtubule-associated protein tau
Channel-proteins (4)			
X78874	0.81	0.19	chloride channel 3
X16645	0.74	0.28	ATPase, Na+/K+ transporting, beta 2 polypeptide
U14419	0.67	0.14	gamma-aminobutyric acid (GABA-A) receptor, subunit beta 2
U16959	0.65	0.15	FK506 binding protein 5 (51 kDa)
Defense (2)			
X06454	0.73	0.24	complement component 4 (within H-2S)
X66295	0.53	0.11	complement component 1, q subcomponent, c polypeptide
Ca-metabolism (2)			
X87142	0.83	0.33	calcium/calmodulin-dependent protein kinase II alpha
AI842328	0.82	0.58	calmodulin 3
Growth factors (1)			
X55573	−0.73	0.23	brain-derived neurotrophic factor
Chaperones (1)			
M20567	0.97	0.31	heat shock protein, 70 kDa 2
Signal transduction (13)			
U50413	1.53	0.92	phosphatidylinositol 3-kinase, regulatory subunit, polypeptide 1 (p85 alpha)
AF022992	1.04	0.13	period homolog 1 (*Drosophila*)
AI838022	0.89	0.31	ADP-ribosylation factor 3
AI849333	0.75	0.17	cerebellar postnatal development protein 1
X84239	0.74	0.14	RAB5B, member RAS oncogene family
AW125157	0.7	0.1	F-box and WD-40 domain protein 1B
AB005654	0.7	0.14	mitogen-activated protein kinase kinase 7
M97516	0.69	0.11	
AA822412	0.68	0.27	RIKEN cDNA 2610313E07 gene

Table 1a (*continued*)

GenBank ID	slr—Average	slr—S.D.	Gene-information
Signal transduction (13)			
AF001871	0.66	0.13	pleckstrin homology, Sec7 and coiled/coil domains 3
D87902	0.62	0.17	ADP-ribosylation factor 5
AI840130	−0.56	0.15	Src activating and signaling molecule
AV280750	−0.56	0.14	mitogen-activated protein kinase 10
Protein degradation (10)			
AW125800	1.18	0.35	ESTs, weakly similar to ubiquitin specific protease 8; putative deubiquitinating enzyme [*Mus musculus*] [*M. musulus*]
L21768	0.83	0.13	epidermal growth factor receptor pathway substrate 15
X57349	0.65	0.11	transferrin receptor
AW050342	0.5	0.09	ubiquitin specific protease 21
AI849361	−0.54	0.12	RIKEN cDNA 1700056O17 gene
AI838853	−0.59	0.08	ubiquitin carboxyl-terminal esterase L5
AI839363	−0.65	0.17	eukaryotic translation initiation factor 3, subunit 6 48-kDa
AI846787	−0.67	0.22	Vhlh-interacting deubiquitinating enzyme 1
AI842835	−0.7	0.09	RIKEN cDNA 1500004O06 gene
AI839225	−0.86	0.17	leucine aminopeptidase 3
Membrane-transport (4)			
AF064748	1.56	0.7	plasma membrane associated protein, S3-12
M22998	1.13	0.27	solute carrier family 2 (facilitated glucose transporter), member 1
M75135	0.89	0.32	solute carrier family 2 (facilitated glucose transporter), member 3
AI843448	0.84	0.36	microsomal glutathione *S*-transferase 3
Transcription-regulation (12)			
M36514	1.19	0.26	zinc finger protein 26
AB021491	0.92	0.32	staphylococcal nuclease domain containing 1
M61007	0.96	0.23	CCAAT/enhancer binding protein (C/EBP), beta
M62362	0.81	0.04	CCAAT/enhancer binding protein (C/EBP), alpha
AI850638	0.65	0.13	thyrotroph embryonic factor
U47543	0.62	0.23	Ngfi-A binding protein 2
X61800	0.51	0.14	CCAAT/enhancer binding protein (C/EBP), delta
U16322	−0.56	0.1	transcription factor 4
AF034745	−0.63	0.17	ligand of numb-protein × 1
Z67747	−0.65	0.13	zinc finger protein 62
AI843959	−0.66	0.25	RIKEN cDNA 5730403B10 gene
X94127	−0.94	0.14	SRY-box containing gene 2
Others and non-classified (21)			
AI851703	1.31	0.47	expressed sequence AW049671
AW227650	1.25	0.26	RIKEN cDNA 0610038P07 gene
AI877157	1.21	0.41	transmembrane 4 superfamily member 9
AF058799	1.14	0.31	3-monooxgenase/tryptophan 5-monooxgenase activation protein, gamma polypeptide

Table 1a (*continued*)

GenBank ID	slr—Average	slr—S.D.	Gene-information
Others and non-classified (21)			
X02801	1	0.53	glial fibrillary acidic protein
D85785	0.92	0.07	protein tyrosine phosphatase, non-receptor type substrate 1
U75321	0.72	0.32	ATPase, aminophospholipid transporter (APLT), class I, type 8A, member 1
AF042180	0.67	0.17	testis-specific protein, Y-encoded-like
AW124835	0.59	0.05	similar to *S*-adenosylmethionine synthetase gamma form (Methionine adenosyltransferase) (AdoMet synthetase) (MAT-II)
AI835481	0.57	0.15	beta-1,3-glucuronyltransferase 3 (glucuronosyltransferase I)
AB033168	0.56	0.23	ZAP3 protein
U51167	0.56	0.03	isocitrate dehydrogenase 2 (NADP+), mitochondrial
X66091	0.54	0.08	*M. musculus* ASF mRNA
AW212859	−0.53	0.12	axotrophin
AI843662	−0.53	0.2	stromal membrane-associated protein
AW046672	−0.53	0.08	DNA segment, Chr 11, ERATO Doi 603, expressed
L00993	−0.53	0.13	Sjogren syndrome antigen B
AW124329	−0.54	0.14	RIKEN cDNA 4921531G14 gene
AI844469	−0.56	0.13	RIKEN cDNA 0610012D09 gene
M34896	−0.56	0.14	ecotropic viral integration site 2
U95498	−0.67	0.22	ALL1-fused gene from chromosome 1q

of zero would indicate no change. Categorization was based on the NetAffx database (http://www.NetAffx.com) [22]. For unsupervised, hierarchical cluster analysis, the Genesis software was used [39].

3. Results

In order to gain insight into the complex expression pattern of mice with a disturbed protein degradation pathway, microarrays representing 12,000 genes were hybridized with labelled RNA isolated from whole brain tissue of 3-month-old male gad mice and compared to two wildtype littermates of the same age. Thus, six comparisons of the expression pattern were achieved. The complete raw data set is publicly available and can be requested directly from the authors. We called a gene (a) stringent differentially regulated when at least six of the six comparisons revealed similar results or (b) moderate differentially regulated when five of six comparisons showed similar results. For both stringencies, genes with an expression difference of at least 1.4-fold (Signal Log Ratio of 0.5) between gad and wildtype mice were considered as significant.

The criteria for stringent differentially regulated genes (Table 1a) were fulfilled by 76 genes with known or putative function and by four ESTs with unknown function. Fifty seven of the genes were up-regulated, whereas

Table 1b
List of moderate differentially regulated genes

GenBank ID	slr—Average	slr—S.D.	Gene-information
RNA-metabolism (4)			
AA791742	1.09	0.28	ARP2 actin-related protein 2 homolog (yeast)
AA690583	0.87	0.34	splicing factor proline/glutamine rich (polypyrimidine tract binding protein associated)
U93050	0.77	0.43	poly(A) binding protein, nuclear 1
AI843586	0.72	0.21	splicing factor, arginine/serine rich 9 (25 kDa)
Vesicle-transport-proteins (4)			
U60150	0.8	0.24	vesicle-associated membrane protein 2
AB025218	0.71	0.11	coated vesicle membrane protein
D12713	0.68	0.15	SEC23A (*S. cerevisiae*)
U91933	0.64	0.3	adaptor-related protein complex AP-3, sigma 2 subunit
Cellular structure proteins (6)			
AF067180	1	0.16	kinesin family member 5C
U51204	0.6	0.19	expressed sequence AI790651
AB023656	0.6	0.21	kinesin heavy chain member 1B
M21041	0.73	0.21	microtubule-associated protein 2
X61399	0.69	0.4	MARCKS-like protein
M18775	−0.69	0.22	microtubule-associated protein tau
Channel-proteins (10)			
X78874	0.81	0.19	chloride channel 3
X16645	0.74	0.28	ATPase, Na+/K+ transporting, beta 2 polypeptide
U43892	0.7	0.16	ATP-binding cassette, subfamily B (MDR/TAP), member 7
U14419	0.67	0.14	gamma-aminobutyric acid (GABA-A) receptor, subunit beta 2
Y17393	0.66	0.24	prefoldin 2
U16959	0.65	0.15	FK506 binding protein 5 (51 kDa)
D10028	0.55	0.2	glutamate receptor, ionotropic, NMDA1 (zeta 1)
D50032	0.51	0.2	trans-golgi network protein 2
U73625	0.51	0.11	transient receptor potential cation channel, subfamily C, member 1
Defense (3)			
X06454	0.73	0.24	complement component 4 (within H-2S)
AW050268	0.64	0.19	HLA-B associated transcript 2
X66295	0.53	0.11	complement component 1, q subcomponent, c polypeptide
Lipid-metabolism (3)			
M91458	−0.53	0.7	sterol carrier protein 2, liver
AB017026	−0.54	0.19	oxysterol binding protein-like 1A
AI845798	−0.6	0.35	RIKEN cDNA 2310004B05 gene
Ca-metabolism (2)			
X87142	0.83	0.33	calcium/calmodulin-dependent protein kinase II alpha
AI842328	0.82	0.58	calmodulin 3
Growth factors (2)			
U42384	−0.65	0.25	fibroblast growth factor inducible 15
X55573	−0.73	0.23	brain-derived neurotrophic factor

(continued on next page)

Table 1b (*continued*)

GenBank ID	slr—Average	slr—S.D.	Gene-information
Chromatin-structure (2)			
M25773	0.7	0.33	SWI/SNF related, matrix associated, actin-dependent regulator of chromatin, subfamily d, member 1
AA794509	0.64	0.27	SWI/SNF-related, matrix-associated, actin-dependent regulator of chromatin, subfamily a, member 5
Chaperones (2)			
D85904	−0.56	0.16	heat shock 70 kDa protein 4
M20567	0.97	0.31	heat shock protein, 70 kDa 2
Signal transduction (25)			
U50413	1.53	0.92	phosphatidylinositol 3-kinase, regulatory subunit, polypeptide 1 (p85 alpha)
AF077660	1.26	0.23	homeodomain interacting protein kinase 3
AF022992	1.04	0.13	period homolog 1 (*Drosophila*)
AI838022	0.89	0.31	ADP-ribosylation factor 3
M63659	0.88	0.46	guanine nucleotide binding protein, alpha 12
U29055	0.77	0.32	guanine nucleotide binding protein, beta 1
AI849333	0.75	0.17	cerebellar postnatal development protein 1
X84239	0.74	0.14	RAB5B, member RAS oncogene family
AW125157	0.7	0.1	F-box and WD-40 domain protein 1B
AB005654	0.7	0.14	mitogen-activated protein kinase kinase 7
AI645561	0.69	0.28	NMDA receptor-regulated gene 1
M97516	0.69	0.11	
AA822412	0.68	0.27	RIKEN cDNA 2610313E07 gene
AF001871	0.66	0.13	pleckstrin homology, Sec7 and coiled/coil domains 3
AA982714	0.64	0.36	adrenergic receptor kinase, beta 1
AF054623	0.62	0.17	frizzled homolog 1, (*Drosophila*)
D87902	0.62	0.17	ADP-ribosylation factor 5
AF014371	0.61	0.18	ras homolog gene family, member A2
AI450876	0.59	0.17	*Mus musculus*, similar to pyridoxal kinase, clone MGC:29261 IMAGE:5064695, mRNA, complete cds
AJ001418	0.57	0.1	pyruvate dehydrogenase kinase, isoenzyme 4
L25674	0.56	0.19	nuclear receptor subfamily 2, group F, member 6
AI840130	−0.56	0.15	Src activating and signaling molecule
AV280750	−0.56	0.14	mitogen-activated protein kinase 10
U20238	−0.56	0.12	RAS p21 protein activator 3
AV370035	−0.73	0.23	chemokine (C–C) receptor 5
Protein degradation (12)			
AW125800	1.18	0.35	ESTs, weakly similar to ubiquitin specific protease 8; putative deubiquitinating enzyme [*Mus musculus*] [*M. musulus*]
L21768	0.83	0.13	epidermal growth factor receptor pathway substrate 15

Table 1b (*continued*)

GenBank ID	slr—Average	slr—S.D.	Gene-information
Protein degradation (12)			
AI853269	0.66	0.27	proteasome (prosome, macropain) subunit, beta type 2
X57349	0.65	0.11	transferrin receptor
M97216	0.59	0.28	amyloid beta (A4) precursor-like protein 2
AW050342	0.5	0.09	ubiquitin specific protease 21
AI849361	−0.54	0.12	RIKEN cDNA 1700056O17 gene
AI838853	−0.59	0.08	ubiquitin carboxyl-terminal esterase L5
AI839363	−0.65	0.17	eukaryotic translation initiation factor 3, subunit 6 48-kDa
AI846787	−0.67	0.22	Vhlh-interacting deubiquitinating enzyme 1
AI842835	−0.7	0.09	RIKEN cDNA 1500004O06 gene
AI839225	−0.86	0.17	leucine aminopeptidase 3
Membran-transport (5)			
AF064748	1.56	0.7	plasma membrane associated protein, S3–12
M22998	1.13	0.27	solute carrier family 2 (facilitated glucose transporter), member 1
AB035174	1.03	0.48	sialytransferase 7 ((alpha-*N*-acetylneuraminyl 2,3-betagalactosyl-1,3)-*N*-acetyl galactosaminide alpha-2, 6-sialytransferase) F
M75135	0.89	0.32	solute carrier family 2 (facilitated glucose transporter), member 3
AI843448	0.84	0.36	microsomal glutathione *S*-transferase 3
Transcription-regulation (22)			
M36514	1.19	0.26	zinc finger protein 26
AB021491	0.92	0.32	staphylococcal nuclease domain containing 1
M88299	1.11	0.5	
M61007	0.96	0.23	CCAAT/enhancer binding protein (C/EBP), beta
M62362	0.81	0.04	CCAAT/enhancer binding protein (C/EBP), alpha
AF015881	0.73	0.13	
AI850638	0.65	0.13	thyrotroph embryonic factor
U47543	0.62	0.23	Ngfi-A binding protein 2
AF064553	0.58	0.25	nuclear receptor-binding SET-domain protein 1
AF084480	0.54	0.19	bromodomain adjacent to zinc finger domain, 1B
X61800	0.51	0.14	CCAAT/enhancer binding protein (C/EBP), delta
X72310	−0.5	0.18	transcription factor Dp 1
L10426	−0.52	0.24	ets variant gene 1
D38046	−0.55	0.19	topoisomerase (DNA) II beta
U16322	−0.56	0.1	transcription factor 4
U07861	−0.59	0.15	zinc finger protein 101
AF034745	−0.63	0.17	ligand of numb-protein × 1
Z67747	−0.65	0.13	zinc finger protein 62
AI843959	−0.66	0.25	RIKEN cDNA 5730403B10 gene
AI957030	−0.66	0.33	RIKEN cDNA 2310001H12 gene
AI851230	−0.76	0.12	RIKEN cDNA 2310035M22 gene
X94127	−0.94	0.14	SRY-box containing gene 2

Table 1b (*continued*)

GenBank ID	slr—Average	slr—S.D.	Gene-information
Others and non-classified (44)			
AI851703	1.31	0.47	expressed sequence AW049671
AW227650	1.25	0.26	RIKEN cDNA 0610038P07 gene
AI877157	1.21	0.41	transmembrane 4 superfamily member 9
AF058799	1.14	0.31	3-monooxgenase/tryptophan 5-monooxgenase activation protein, gamma polypeptide
X02801	1	0.53	glial fibrillary acidic protein
D85785	0.92	0.07	protein tyrosine phosphatase, non-receptor type substrate 1
M93310	0.86	0.76	metallothionein 3
U52824	0.81	0.17	tubby
AI646638	0.79	0.15	*Mus musculus*, clone MGC:37615 IMAGE:4989784, mRNA, complete cds
AF006466	0.79	0.03	formin-like
AW227650	0.77	0.22	RIKEN cDNA 0610038P07 gene
U75321	0.72	0.32	ATPase, aminophospholipid transporter (APLT), class I, type 8A, member 1
AF039833	0.69	0.39	contactin associated protein 1
AF042180	0.67	0.17	testis-specific protein, Y-encoded-like
U62673	0.62	0.12	
AI849718	0.6	0.2	RIKEN cDNA 1500010B24 gene
AA414964	0.6	0.2	ESTs, Weakly similar to ATY1_MOUSE Probable cation-transporting ATPase 1 [*M. musulus*]
AW124835	0.59	0.05	similar to *S*-adenosylmethionine synthetase gamma form (Methionine adenosyltransferase) (AdoMet synthetase) (MAT-II)
AF076482	0.57	0.17	peptidoglycan recognition protein
AI835481	0.57	0.15	beta-1,3-glucuronyltransferase 3 (glucuronosyltransferase I)
AB033168	0.56	0.23	ZAP3 protein
U51167	0.56	0.03	isocitrate dehydrogenase 2 (NADP+), mitochondrial
AW124101	0.55	0.08	expressed sequence AA408278
X66091	0.54	0.08	*M. musculus* ASF mRNA
U11075	0.54	0.13	potassium inwardly-rectifying channel, subfamily J, member 4
D00472	0.51	0.15	cofilin 1, non-muscle
AJ006587	0.5	0.16	eukaryotic translation initiation factor 2, subunit 3, structural gene X-linked
AW048159	0.5	0.1	RIKEN cDNA 1200017E04 gene
AW212859	−0.53	0.12	axotrophin
AI843662	−0.53	0.2	stromal membrane-associated protein
AW046672	−0.53	0.08	DNA segment, Chr 11, ERATO Doi 603, expressed
L00993	−0.53	0.13	Sjogren syndrome antigen B
AW124044	−0.53	0.06	protein-L-isoaspartate (D-aspartate) *O*-methyltransferase 1
AW124329	−0.54	0.14	RIKEN cDNA 4921531G14 gene
AA839379	−0.55	0.14	RIKEN cDNA 2610002J02 gene
AI504338	−0.56	0.2	ESTs
AI844469	−0.56	0.13	RIKEN cDNA 0610012D09 gene
M34896	−0.56	0.14	ecotropic viral integration site 2
U83174	−0.57	0.22	gene trap ROSA 26, Philippe Soriano
AI853444	−0.59	0.22	RIKEN cDNA 2610042L04 gene
AA623587	−0.6	0.1	expressed sequence AA536743
U95498	−0.67	0.22	ALL1-fused gene from chromosome 1q

23 genes were down-regulated in the *gad* mice. These genes can be grouped according to their function (Table 1a) into RNA metabolism (3 up- and 0 down-regulated, 3/0), vesicle transport (3/0), proteins of the cell structure (3/1), channel proteins (4/0), calcium metabolism (2/0), growth factors (0/1), chaperones (1/0), signal transduction (11/2), membrane transport (4/0), transcription regulation (7/5), and others or unknown function (13/8). Nearly no gene of the immune-related proteins was found to be differentially regulated (2/0).

The criteria for moderate regulated genes were fulfilled by 134 genes with known or putative function and 12 ESTs without known function. A total of 103 of the genes were up-regulated, whereas 43 genes were down-regulated in the *gad* mice. These genes can be grouped according to their function (Table 1b) into RNA metabolism (4 up- and 0 down-regulated, 4/0), vesicle transport (4/0), proteins of the cell structure (5/1), defense (3/0), channel proteins (10/0), Lipid metabolisms (0/3), calcium metabolism (2/0), growth factors (0/2), chromatin structure (2/0), chaperones (1/1), signal transduction (21/4), membrane transport (5/0), transcription regulation (11/11), and others or unknown function (30/14).

Of the protein degradation pathway, six genes were down-regulated and another four genes were found to be up-regulated (Table 1a). Our first hypothesis that genes of the UCH gene family might compensate for the lack of UCH-L1 function was not confirmed. In contrast, UCH-L5 was found to be down-regulated.

At a first look, UCH-L1 was not differentially expressed. The reduction of the signal by the deletion of exons 7 and 8 is too weak for a change call of the Affymetrix software. However, the appropriate oligos show the absence of the corresponding RNA regions (data not shown).

An unsupervised, hierarchical cluster algorithm allowed us to cluster the five analyzed brains on the basis of their similarities measured over these 146 significant regulated genes from Table 1b (Fig. 1). In the dendrogram shown in Fig. 1 (left and top), the length and the subdivision of the branches display the relatedness of the brains (top) and the expression of the genes (left). Two distinct groups of brains (3 KO and 2 wt brains) and two groups of genes are shown.

4. Discussion

Ubiquitin has been implicated in numerous processes of the cell including cell-cycle control, receptor function,

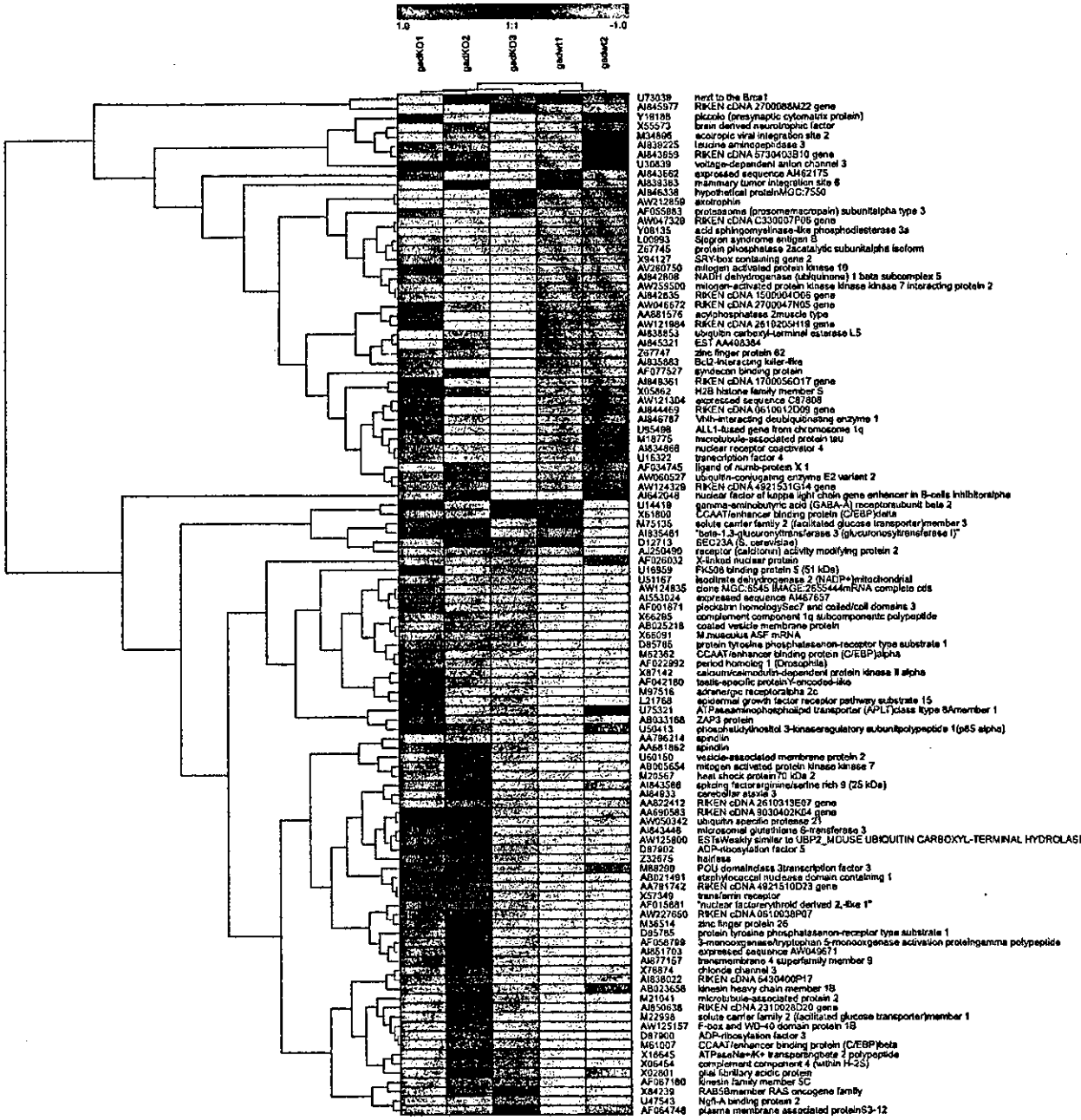

Fig. 1. Unsupervised two-dimensional cluster analysis of transcript ratios for the five mice brains (3 KO and 2 wt brains). There were 146 significant genes across the group. Each row represents a single gene and each column one brain. As shown in the colour bar, red indicates up-regulation, green down-regulation, black no change, and grey no data available.

signalling pathways, antigen presentation, degradation of proteins, and regulation of transcription. Analogous to these functions, alteration of the ubiquitin pathway will affect several of these pathways which may not be identifiable by single gene analysis. To investigate the complex network of gene regulation, we analyzed the expression pattern of 12,000 genes in 3-month-old male Uch-l1 deficient (*gad*) mice. This age was described to present the progressive phase of the disease [13]. The mutant mice used for this study showed sensory ataxia and motor paresis. Significant expression changes were found in more then 146 genes (Tables 1a and b). As expected, these genes are involved in several pathways of protein degradation, transcription regulation, vesicle and membrane transport, and signal transduction.

The gene most significantly down-regulated in the gad mice was Sox2 also known as SRY-box containing gene 2 (Signal log ratio −0.94, S.D. 0.14). Mutations of SOX2 cause anophthalmia in humans [9]. In mice, inactivation of Sox2 suggested a role in embryonal implantation [1]. SOX2

has been implicated in the regulation of Fgf4 expression [1]. In our experiments, we found no indication for a differential regulation of Fgf4, however, the inducible Fgf15 was down-regulated in *gad* mice (−0.65, S.D. 0.25) suggesting a role of Sox2 in Fgf15 expression and indicating a complex expression regulation mechanism of the Fgf gene family. Fgfs have been defined as regulators of the central nervous development and function (reviewed in Ref. [7]). However, the functional implication of a down-regulation of Fgf15 in mice has not been explored yet. Therefore, gad mice might suit as a model to study Fgf15 in more detail. Cofactors of Sox2 are totally unknown. One could speculate that transcription factors acting partially synergistic with Sox2 might be up-regulated in gad mice. In fact, we found several up-regulated transcription factors such as the eukaryotic translation initiation factor 2 (0.5, S.D. 0.16), the zinc finger protein 26 (1.19, S.D. 0.26), and CCAAT/enhancer binding protein (0.96, S.D. 0.23), respectively. Most convincingly, mRNAs of the alpha, beta, and delta subunits of the CCAAT/enhancer binding protein (C/EBP) were increased, respectively. Fig. 2 shows the central role of C/EBP. More than 20 adjusted genes can be implemented on a coherent biochemical network. For example, C/EBPs provide another link to the above-mentioned Fgf expression changes as a C/EBP site is an important regulatory element for FGF-binding protein activity [14]. Early changes of expression of C/EBP beta were also observed in other neurodegenerative diseases [21]. Most interestingly, only the inhibitory gamma and zeta subunits of C/EBP but not the positively functioning beta subunit have been found to be multi-ubiquinated and degraded by the proteasome [11]. We also found mRNA encoding the homeodomain interacting protein kinase 3 (HIPK3) to be up-regulated (1.26, S.D. 0.23). HIPK3 belongs to a family of co-repressors that potentiate the transcriptional activities of homeoproteins [16]. In gad mice, we found the homeobox gene containing transcription factor paired box gene 6 down-regulated (−0.44, S.D. 0.12). However, whether interaction of HIPK3 to the paired box gene 6 or other transcription factors as Sox2 is part of transcription activation has not been shown yet. Interestingly though, mutations in the paired box gene 6 causes eye diseases as mutations in Sox 2 [9]. How UCH-L1 is implicated in this process needs to be defined. For gad mice, however, abnormal eye development has not been described. It is likely that complete loss of function but no small alterations of the expression levels of these genes lead to the described developmental alterations. In gad mice, several other transduction pathways seem to be altered including the phosphatidylinositol 3 kinase (PI3K) pathway which is also linked to C/EBP. Specifically, the p85 alpha subunit of PI3K was found to be up-regulated (1.53; S.D. 0.92) (Fig. 2).

Besides the above-mentioned reduction of fgf15 mRNA, the brain-derived neurotrophic factor (BDNF) is also reduced in gad mice (−0.73, S.D. 0.23). BDNF has been reported to act on motor neurons [12] and to stimulate developmental neuro-muscular synapses [24]. Although BDNF reduction has not been reported yet in gad mice, one of us found significantly reduced NGF levels primarily in the spinal cord but not in the brain [29]. It has to be mentioned that spinal cord was not analyzed in our Chip analyses. However, in gad mice, decreased muscle weight has been observed with age which could be caused by the reduced BDNF and/or fgf15 levels, respectively. Although the function of another trophin, axotrophin, needs still to be explored, a reduction (−0.53, S.D. 0.12) of this factor implicates its significance in neuronal survival. In agreement with this hypothesis, Haendel and colleagues found neuronal degeneration in axotrophin-deficient mice (NCBI link NM_020575). In contrast, epidermal growth factor

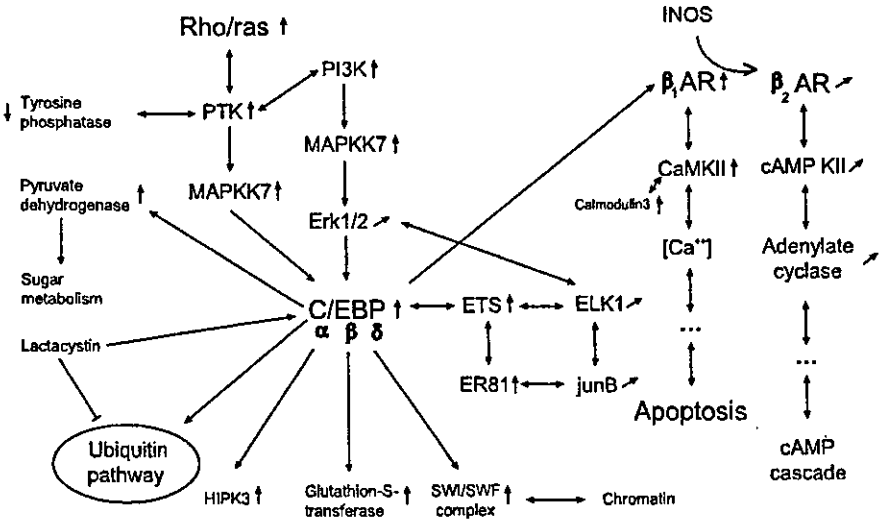

Fig. 2. C/EBP pathway demonstrating interactions of proteins which transcripts are differentially regulated in gad mice (up-regulated in six of six comparisons marked with ↑, upregulated genes in five or six of six comparisons are indicated with /, down-regulated in six of six comparisons are indicated with ↓).

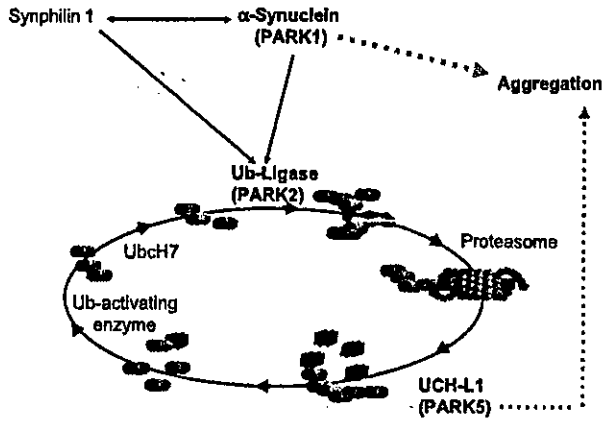

Fig. 3. Scheme of proteins altered in Parkinson's disease which place UCH-L1 as part of the altered protein degradation pathway and highlight the role of investigating Uch-l1-deficient (gad) mice by expression analysis.

receptor pathway substrate 15 was increased (0.83, S.D. 0.13) and might indicate a regulatory mechanism of gad mice trying to prevent neuronal degeneration.

Pathological features of gad mice are spheroid dystrophic axons dying back the dorsal root ganglia (DRG) progressing along the gracile tract of the spinal cord towards the parental neurons [15]. Immunohistochemically, almost all of the primary neurons and of the glial cells in DRG of gad mice revealed strong amyloid precursor protein (APP) staining [13]. The authors hypothesized abnormal expression of APP in gad mice as the cause of the pathological features. Although increased APP transcript in the brain has not been confirmed by our transcription analysis, amyloid beta (A4) precursor-like protein 2 was upregulated (0.59, S.D. 0.28). Our data also define an up-regulation of glial fibrillary acidic protein (GFAP) as the cause of the increased immunoreactivity of GFAP in astrocytes of gad mice [44].

We were in particular interested in genes involved in protein degradation. We hypothesized to find genes encoding proteins with UCH-L1 complementary functions compensatory up-regulated. Fig. 3 shows a simplified scheme of ubiquitin-altered protein degradation in PD and the task of UCH-L1. However, only the beta type 2 proteasome (prosome, macropain) subunit (0.66, S.D. 0.27) and the ubiquitin specific protease 21 (0.5, S.D. 0.09) were found to be increased. Interestingly, ubiquitin C-terminal hydrolase activity is associated with the 26S protease complex [8]. However, a direct interaction between UCH-L1 and macropain remains to be shown. Furthermore, Hsp70 protein 2 was increased (0.97, S.D. 0.31) likely due to decreased proteasomal degradation of proteins in gad mice, whereas Hsp70 protein 4 was down-regulated (−0.56, S.D. 0.16). Ubiquitin carboxyl-terminal esterase L5 was also significantly decreased (−0.59, S.D. 0.08).

In summary, the alteration of many pathways in gad mice offers an interesting mouse model which needs to be studied in more detail. The development of genome wide transcription profiles of mouse models in general will help to decipher the interaction and dependence of genes and gene products in their complexity of a living organism. Although it is not clear yet whether this complexity of biology in development, health and disease into their final details will be completely understood, a first step is being done to explore normal variation and disease processes at the RNA level using microarray chip analyses.

Acknowledgements

The authors thank D. Berg for the helpful discussions. This work was supported by a grant from the Federal Ministry of Education and Research (Fö. 01KS9602) and the Interdisciplinary Center of Clinical Research Tübingen (IZKF). Work of K.W. was supported by the grant for Research on Brain Science from the Ministry of Health, Labour and Welfare of Japan, Grants-in-Aid for Scientific Research from the Ministry of Education, Culture, Sports, Science and Technology of Japan, grants from the Organization for Pharmaceutical Safety and Research, and a grant from Japan Science and Technology Cooperation.

References

[1] A.A. Avilion, S.K. Nicolis, L.H. Pevny, L. Perez, N. Vivian, R. Lovell-Badge, Multipotent cell lineages in early mouse development depend on SOX2 function, Genes Dev. 17 (2003) 126–140.
[2] M.C. Bennett, J.F. Bishop, Y. Leng, P.B. Chock, T.N. Chase, M.M. Mouradian, Degradation of alpha-synuclein by proteasome, J. Biol. Chem. 274 (1999) 33855–33858.
[3] K.K.K. Chung, Y. Zhang, K.L. Lim, Y. Tanaka, H. Huang, J. Gao, et al., Parkin ubiquitinates the α-synuclein-interacting protein, synphilin-1: implications for Lewy-body formation in Parkinson disease, Nat. Med. 7 (2001) 1144–1150.
[4] A. Ciechanover, A.L. Schwartz, The ubiquitin–proteasome pathway: the complexity and myriad functions of proteins death, Proc. Natl. Acad. Sci. U. S. A. 95 (1998) 2727–2730.
[5] I.N. Day, L.J. Hinks, R.J. Thompson, The structure of the human gene encoding protein gene product 9.5 (PGP9.5), a neuron-specific ubiquitin C-terminal hydrolase, Biochem. J. 268 (1990) 521–524.
[6] M.C. DeRijk, C. Tzourio, M.M.B. Breteler, J.F. Dartigues, L. Amaducci, S. Lopez-Pousa, et al., Prevalence of parkinsonism and Parkinson's disease in Europe: the EUROPARKINSON collaborative study, J. Neurol. Neurosurg. Psychiatry 62 (1997) 10–15.
[7] R. Dono, Fibroblast growth factors as regulators of central nervous system development and function, Am. J. Physiol., Regul. Integr. Comp. Physiol. 284 (2003) R867–R881.
[8] E. Eytan, T. Armon, H. Heller, S. Beck, A. Hershko, Ubiquitin C-terminal hydrolase activity associated with the 26S protease complex, J. Biol. Chem. 268 (1993) 4668–4674.
[9] J. Fantes, N.K. Ragge, S.A. Lynch, N.I. McGill, J.R. Collin, P.N. Howard-Peebles, C. Hayward, A.J. Vivian, K. Williamson, V. Van Heyningen, D.R. Fitz Patrick, Mutations in SOX2 cause anophthalmia, Nat. Genet. 33 (2003) 461–463.
[10] L.I. Golbe, G. Di Iorio, G. Sanges, A.M. Lazzarini, S. La Salsa, V. Bonavita, et al., Clinical genetic analysis of Parkinson's disease in the Contursi kindred, Ann. Neurol. 40 (1996) 767–775.
[11] T. Hattori, N. Ohoka, Y. Inoue, H. Hayashi, K. Onozaki, C/EBP family transcription factors are degraded by the proteasome but stabilized by forming dimmer, Oncogene 22 (2003) 1273–1280.

[12] C.E. Henderson, W. Camu, C. Mettling, A. Gouin, K. Poulsen, M. Karihaloo, J. Ruliamas, T. Evans, S.B. McMahon, M.P. Armanini, L. Berkemeier, H.S. Phillips, A. Rosenthal, Neurotrophins promote motor neuron survival and are present in embryonic limb bud, Nature 364 (1993) 266–270.
[13] N. Ichihara, J. Wu, D.H. Chui, K. Yamazaki, T. Wakabayashi, T. Kikuchi, Axonal degeneration promotes abnormal accumulation of amyloid beta-protein in ascending gracile tract of gracile axonal dystrophy (GAD) mouse, Brain Res. 695 (1995) 173–178.
[14] B.L. Kagan, R.T. Henke, R. Cabal-Manzano, G.E. Stoica, Q. Nguyen, A. Wellstein, A.T. Riegel, Complex regulation of the fibroblast growth factor-binding protein in MDA-MB-468 breast cancer cells by CCAAT/Enhancer-binding protein beta, Cancer Res. 63 (2003) 1696–1705.
[15] T. Kikuchi, M. Mukoyama, K. Yamazaki, H. Moriya, Axonal degeneration of ascending sensory neurons in gracile axonal dystrophy mutant mouse, Acta Neuropathol. 80 (1990) 145–151.
[16] Y.H. Kim, C.Y. Choi, S.-J. Lee, M.A. Conti, Y. Kim, Homeodomain-interacting protein kinases, a novel family of co-repressors for homeodomain transcription factors, J. Biol. Chem. 273 (1998) 25875–25879.
[17] T. Kitada, S. Asakawa, N. Hattori, H. Matsumine, Y. Yamamura, S. Minoshima, et al., Mutations in the parkin gene cause autosomal recessive juvenile parkinsonism, Nature (London) 392 (1998) 605–608.
[18] R. Kruger, W. Kuhn, T. Muller, D. Woitalla, M. Graeber, S. Kosel, H. Przuntek, J.T. Epplen, L. Schols, O. Riess, Ala30Pro mutation in the gene encoding alpha-synuclein in Parkinson's disease, Nat. Genet. 18 (1998) 106–108.
[19] R. Kruger, O. Eberhardt, O. Riess, J.B. Schulz, Parkinson's disease: one biochemical pathway to fit all genes? Trends Mol. Med. 8 (2002) 236–240.
[20] E. Leroy, R. Boyer, G. Auburger, B. Leube, G. Ulm, E. Mezey, G. Brownstein, M.J. Brownstein, S. Jonnalagada, T. Chernova, et al., The ubiquitin pathway in Parkinson's disease, Nature 395 (1998) 451–452.
[21] A.P. Lieberman, G. Harmison, A.D. Strand, J.M. Olson, K.H. Fischbeck, Altered transcriptional regulation in cells expressing the expanded polyglutamine androgen receptor, Hum. Mol. Genet. 11 (2002) 1967–1976.
[22] G. Liu, A.E. Loraine, R. Shigeta, M. Cline, J. Cheng, V. Valmeekam, S. Sun, D. Kulp, M.A. Siani-Rose, NetAffx: affymetrix probesets and annotations, Nucleic Acids Res. 31 (2003) 82–86.
[23] Y. Liu, L. Fallon, H.A. Lashuel, Z. Liu , P.T. Lansbury Jr., The UCH-L1 gene encodes two opposing enzymatic activities that affect alpha-synuclein degradation and Parkinson's disease susceptibility, Cell 111 (2002) 209–218.
[24] A.M. Lohof, Y. Ip, M. Poo, Potentiation of developing neuromuscular synapses by the neurotrophins NT-3 and BDNF, Nature 363 (1993) 350–353.
[25] J. Lowe, H. McDermott, M. Landon, R.J. Mayer, K.D. Wilkinson, Ubiquitin carboxyl-terminal hydrolase (PGP 9.5) is selectively present in ubiquitinated inclusion bodies characteristic of human neurodegenerative diseases, J. Pathol. 161 (1990) 153–160.
[26] C.B. Lücking, A. Dürr, V. Bonifati, J. Vaugham, G. De Michele, T. Gasser, et al., Association between early-onset Parkinson's disease and mutations in the parkin gene, N. Engl. J. Med. 342 (2000) 1560–1567.
[27] D.M. Maraganore, M.J. Farrer, J.A. Hardy, S.J. Lincoln, S.K. McDonnell, W.A. Rocca, Case-control study of the ubiquitin carboxy-terminal hydrolase L1 gene in Parkinson's disease, Neurology 53 (1999) 1858–1860.
[28] F.P. Marx, C. Holzmann, K.M. Strauss, L. Li, O. Eberhard, M. Cookson, et al., Identification and functional characterization of a novel R621C mutation in the synphilin-1 gene in Parkinson's disease, Hum. Mol. Genet. 12 (2003) 1223–1231.
[29] K. Matsui, S. Furukawa, J.-G. Suh, K. Wada, Developmental changes of nerve growth factor levels in the gracile axonal dystrophy mouse, Neurosci. Lett. 177 (1994) 116–118.
[30] K.S. McNaught, L.M. Bjorklund, R. Belizaire, O. Isacson, P. Jenner, C.W. Olanow, Proteasome inhibition causes nigral degeneration with inclusion bodies in rats, NeuroReport 13 (2002) 1437–14411.
[31] D.J. Nicholl, J.R. Vaughan, N.L. Khan, S.L. Ho, D.E.W. Aldous, S. Lincoln, et al., Two large British kindreds with familial Parkinson's disease: a clinico-pathological and genetic study, Brain 125 (2002) 44–57.
[32] K. Nishikawa, H. Li, R. Kawamura, H. Osaka, Y.L. Wang, Y. Hara, et al., Alterations of structure and hydrolase activity of parkinsonism-associated human ubiquitin carboxyl-terminal hydrolase L1 variants, Biochem. Biophys. Res. Commun. 304 (2003) 176–183.
[33] H. Osaka, Y.L. Wang, K. Takada, S. Takizawa, R. Setsuie, H. Li, Y. Sato, et al., Ubiquitin carboxy-terminal hydrolase L1 binds to and stabilizes monoubiquitin in neuron, Hum. Mol. Genet. 12 (2003) 1945–1958.
[34] E. Ozkaynak, D. Finley, M.J. Solomon, A. Varshavsky, The yeast ubiquitin genes: a family of natural gene fusions, EMBO J. 6 (1987) 1429–1439.
[35] P. Piccini, D.J. Burn, R. Ceravolo, D. Maraganore, D.J. Brooks, The role of inheritance in sporadic Parkinson's disease: evidence from a longitudinal study of dopaminergic function in twins, Ann. Neurol. 45 (1999) 577–582.
[36] M.H. Polymeropoulos, C. Lavedan, E. Leroy, S.E. Ide, A. Dehejia, A. Dutra, B. Pike, H. Root, J. Rubenstein, R. Boyer, E.S. Stenroos, S. Chandrasekharappa, A. Athanassiadou, T. Papapetropoulos, W.G. Johnson, A.M. Lazzarini, R.C. Duvoisin, G. Di Iorio, L.I. Golbe, R.L. Nussbaum, Mutation in the alpha-synuclein gene identified in families with Parkinson's disease, Science 276 (1997) 2045–2047.
[37] K. Saigoh, Y.L. Wang, J.G. Suh, T. Yamanishi, Y. Sakai, H. Kiyosawa, T. Harada, N. Ichihara, S. Wakana, T. Kikuchi, K. Wada, Intragenic deletion in the gene encoding ubiquitin carboxy-terminal hydrolase in gad mice, Nat. Genet. 23 (1999) 47–51.
[38] H. Shimura, N. Hattori, S.-I. Kubo, Y. Mizuno, S. Asakawa, S. Minoshima, et al., Familial Parkinson disease gene product, parkin, is a ubiquitin-protein ligase, Nat. Genet. 25 (2000) 302–305.
[39] A. Sturn, J. Quackenbush, Z. Trajanoski, Genesis: cluster analysis of microarray data, Bioinformatics 18 (2002) 207–208.
[40] G.K. Tofaris, R. Layfield, M.G. Spillantini, Alpha-synuclein metabolism and aggregation is linked to ubiquitin-independent degradation by the proteasome, FEBS Lett. 509 (2001) 22–26.
[41] K.D. Wilkinson, K.M. Lee, S. Deshpande, P. Duerksen-Hughes, J.M. Boss, J. Pohl, The neuron-specific protein PGP 9.5 is a ubiquitin carboxyl-terminal hydrolase, Science 246 (1989) 670–673.
[42] P. Wintermeyer, R. Krüger, W. Kuhn, T. Müller, D. Woitalla, D. Berg, et al., Mutation analysis and association studies of the UCHL1 gene in German Parkinson's disease patients, NeuroReport 11 (2000) 2079–2082.
[43] Z.K. Wszolek, B. Pfeiffer, J.R. Fulgham, J.E. Parisi, B.M. Thompson, R.J. Uitti, et al., Western Nebraska family (family-D) with autosomal dominant parkinsonism, Neurology 45 (1995) 502–505.
[44] K. Yamazaki, H. Moriya, N. Ichihara, H. Mitsushio, S. Inagaki, T. Kikuchi, Substance P-immunoreactive astrocytes in gracile sensory nervous tract of spinal cord in gracile axonal dystrophy mutant mouse, Mol. Chem. Neuropathol. 20 (1993) 1–20.

BIOLOGY OF REPRODUCTION 71, 515–521 (2004)
Published online before print 14 April 2004.
DOI 10.1095/biolreprod.104.027565

Developmental Regulation of Ubiquitin C-Terminal Hydrolase Isozyme Expression During Spermatogenesis in Mice

Jungkee Kwon,[2,3] Yu-Lai Wang,[1] Rieko Setsuie,[3,4] Satoshi Sekiguchi,[2] Mikako Sakurai,[3,4] Yae Sato,[3,4] Won-Woo Lee,[2] Yoshiyuki Ishii,[2] Shigeru Kyuwa,[2] Mami Noda,[4] Keiji Wada,[3] and Yasuhiro Yoshikawa[1,2]

Department of Biomedical Science,[2] Graduate School of Agricultural and Life Sciences, University of Tokyo, Bunkyo-ku, Tokyo, 113-8657, Japan
Department of Degenerative Neurological Disease,[3] National Institute of Neuroscience, National Center of Neurology and Psychiatry, Kodaira, Tokyo, 187-8502, Japan
Laboratory of Pathophysiology,[4] Graduate School of Pharmaceutical Sciences, Kyushu University, Higashi-ku, Fukuoka, 812-8582, Japan

ABSTRACT

The ubiquitin pathway functions in the process of protein turnover in eukaryotic cells. This pathway comprises the enzymes that ubiquitinate/deubiquitinate target proteins and the proteasome that degrades ubiquitin-conjugated proteins. Ubiquitin C-terminal hydrolases (UCHs) are thought to be essential for maintaining ubiquitination activity by releasing ubiquitin (Ub) from its substrates. Mammalian UCH-L1 and UCH-L3 are small proteins that share considerable homology at the amino acid level. Both of these UCHs are highly expressed in the testis/ovary and neuronal cells. Our previous work demonstrated that UCH-L1-deficient gracile axonal dystrophy (*gad*) mice exhibit progressively decreasing spermatogonial stem cell proliferation, suggesting that UCH isozymes in the testis function during spermatogenesis. To analyze the expression patterns of UCH isozymes during spermatogenesis, we isolated nearly homogeneous populations of spermatogonia, spermatocytes, spermatids, and Sertoli cells from mouse testes. Western blot analysis detected UCH-L1 in spermatogonia and Sertoli cells, whereas UCH-L3 was detected in spermatocytes and spermatids. Moreover, reverse transcription-polymerase chain reaction analysis of UCH isozymes showed that UCH-L1 and UCH-L4 mRNAs are expressed in spermatogonia, whereas UCH-L3 and UCH-L5 mRNAs are expressed mainly in spermatocytes and spermatids. These results suggest that UCH-L1 and UCH-L3 have distinct functions during spermatogenesis, namely, that UCH-L1 may act during mitotic proliferation of spermatogonial stem cells whereas UCH-L3 may function in the meiotic differentiation of spermatocytes into spermatids.

male reproductive tract, meiosis, Sertoli cells, spermatogenesis, testis

INTRODUCTION

Ubiquitination of proteins is mediated by specific enzymes, namely E1 (ubiquitin-activating), E2 (ubiquitin-conjugating), and E3 (ubiquitin ligase) [1]. In this pathway, polyubiquitinated proteins are translocated to the proteasome and proteolytically degraded in an energy-dependent manner. The ubiquitin pathway plays important roles in regulating numerous cellular processes, including the degradation of intracellular proteins, cell-cycle regulation, stress responses, and programmed cell death [2–6]. Ubiquitin can be released from polyubiquitin chains or ubiquitin-protein conjugates via the action of deubiquitinating enzymes. These enzymes are divided into two families: ubiquitin C-terminal hydrolases (UCHs) and ubiquitin-specific proteases (UBPs). UCHs remove ubiquitin from peptides or small C-terminal ubiquitin adducts only, whereas UBPs are thought to disassemble polyubiquitin chains [7, 8].

Recent studies show that there are at least four mammalian UCH isozymes, among which the residues surrounding the active site share a high degree of homology [8, 9]. Mouse *Uchl1* and *Uchl3* encode proteins of similar size that share 52% amino acid sequence identity [8, 10]. However, the distribution of these isozymes is quite distinct; UCH-L1 mRNA is selectively and highly expressed in the testis/ovary and neuronal cells [10–12], whereas UCH-L3 mRNA is expressed in all tissues, including the testis/ovary and brain [13, 14]. UCH-L1-specific antibodies stain the testis, especially spermatogonia and Sertoli cells [15–18]. In addition, UCH-L1-deficient gracile axonal dystrophy (*gad*) mutant mice exhibit pathological changes, such as progressively decreasing spermatogonial stem cell proliferation [18]. These results led us to postulate that UCH isozymes in the testis function in the development of spermatogonia into mature sperm. Spermatogenesis is a complex, highly organized process that is divided into three phases: proliferation, meiosis, and spermiogenesis [19], each of which may require the activity of specific UCH isozymes. However, our understanding of the functional roles and the localization of UCH isozymes during spermatogenesis is limited.

In the present study, we generated peptide-specific antibodies against sequences within UCH-L1 or UCH-L3 and purified developing sperm cells at each stage from testes using immunomagnetic beads followed by discontinuous Percoll gradient centrifugation [20–23]. We found that the expression level of each UCH isozyme increased during the first round of spermatogenesis, and that the isozymes exhibited differential expression in the mouse testis [24]. Our results suggest that UCH isozymes play an important role in the regulation of spermatogenesis.

[1]Correspondence: Yasuhiro Yoshikawa, Department of Biomedical Science, Graduate School of Agricultural and Life Sciences, University of Tokyo, 1-1-1 Yayoi, Bunkyo-ku, Tokyo 113-8657, Japan.
FAX: 81 3 5841 8186; e-mail: ayyoshi@mail.ecc.u-tokyo.ac.jp

Received: 20 January 2004.
First decision: 5 February 2004.
Accepted: 19 March 2004.

ISSN: 0006-3363. http://www.biolreprod.org

MATERIALS AND METHODS

Animals

The *gad* [11] and *Uchl3* knockout [13] mice were used as controls. The *gad* mouse is an autosomal recessive mutant that was obtained from the cross between CBA and RFM mice. The mutant line was maintained by intercross for more than 20 generations. The *Uchl3* knockout mouse was generated by the standard method using homologously recombinant ES cells from 129SV mice. The knockout line was back-crossed several times to C57BL/6J mice. Male Balb/c mice were purchased from Nihon CLEA, Inc. (Tokyo, Japan), and all animals were maintained at the National Institute of Neuroscience, National Center of Neurology and Psychiatry (Japan).

All mouse experiments were performed in accordance with the institution's regulations for animal care and with the approval of the Animal Investigation Committee.

Isolation of Type A Spermatogonia and Sertoli Cells

Sequential enzymatic digestion of testicular tubules was performed as previously described [21]. After treatment with erythrocyte lysing buffer, testes from ten 2-wk-old and two 8-wk-old Balb/c mice were incubated twice for 5 min at 34°C with medium containing 0.5 mg/ml collagenase IV-S (Sigma-Aldrich, St. Louis, MO) and digested for 10 min at 34°C with medium containing 1 mg/ml trypsin (Sigma-Aldrich).

After the sequential enzymatic digestion, type A spermatogonia were isolated using immunomagnetic beads. The cells were incubated at room temperature for 15 min with biotin-conjugated rat anti-mouse CD117 (1 μg/10^6 cells), which recognizes the extracellular domain of the c-kit receptor (clone 2B8; Pharmingen, San Diego, CA). The cell suspension was then centrifuged at 300 × *g* for 5 min and washed with Dulbecco modified Eagle medium to remove excess antibody. The cell pellet was then resuspended in 80 μl buffer and incubated with 20 μl MACS anti-biotin microbeads (Miltenyi Biotec, Bergisch Gladbach, Germany) per 10^7 total cells at 6–12°C for 15 min. The cell suspension was then washed carefully and resuspended in 500 μl buffer per 10^8 total cells. The c-kit-positive cells (type A spermatogonia) were separated with a MACS separator (Miltenyi Biotec) and collected. The suspension containing Sertoli cells was resuspended at a concentration of 1 × 10^6 cells/ml in tissue culture medium containing 10% fetal calf serum.

Sertoli Cell Culture and Purification

The suspension containing Sertoli cells obtained from testes of ten 2-wk-old mice was plated on lectin- (Datura stramonium agglutinin; Sigma, St. Louis, MO) coated dishes as described [25, 26] and incubated for 3 days at 37°C. Alkaline phosphatase activity was visualized according to the procedure of Cox and Singer [27]. Cultured cells were incubated in reaction buffer (100 mM Tris-HCl, 100 mM NaCl, 50 mM $MgCl_2$, pH 9.5) containing 0.17 mg/ml 5-bromo-4-chloro-3-indolyl phosphate and 0.33 mg/ml nitro blue tetrazolium chloride.

Isolation of Spermatocytes and Spermatids

After isolating type A spermatogonia from testes of 8-wk-old mice using immunomagnetic beads, the testicular cell suspension was separated by discontinuous Percoll (Amersham Biosciences, Piscataway, NJ) gradient centrifugation [20]. The recovered cell populations were analyzed by phase-contrast microscopy [28], fluorescence-activated cell sorting (FACS) [29], and reverse transcription-polymerase chain reaction (RT-PCR).

RT-PCR Analysis of Isolated Cells Expressing Specific Marker Genes

From each population of spermatogonia, spermatocytes, spermatids, and Sertoli cells isolated from testicular cell suspensions, mRNAs were extracted using the QuickPrep micro mRNA purification kit (Amersham Biosciences) and subjected to reverse transcription with a first-strand cDNA synthesis kit (Amersham Biosciences) according to the manufacturer's instructions. PCR was performed with the following primers; c-kit [30], 5′-AAGATTTGCGATTTCGGGC-3′ and 5′-CTGAAAATGCTCTC TGGTGCC-3′; Histone H1t [7], 5′-GTCCAGCTCTTGACCATGTCG-3′ and 5′-GCTTTTTCCCTCGCCTTTTAG-3′; SP-10 [31], 5′-TTTATCTG CTTGGATCTGCCC-3′, and 5′-GCTTGAAAGTTGCTGAACCG-3′; stem cell factor (SCF) [32], 5′-ATAGGAAAGCCGCAAAGGC-3′ and 5′-TTACAAGCGAAATGAGAGCCG-3′; and glyceraldehyde-3-phosphate dehydrogenase [33]. Each sample was amplified using the AmpliTaq Gold GeneAmp system (Applied Biosystems, Foster City, CA).

FACS Analysis of Isolated Cells

FACS analysis was performed as described by Malkove et al. [29, 34]. Briefly, isolated spermatogenic cells were fixed in 70% ethanol overnight at 4°C and then incubated in propidium iodide staining solution (50 μg/ml and 100 U/ml RNase A in PBS) for 30 min at room temperature. Within 2 h poststaining, the isolated spermatogenic cells were analyzed by FACS (FACSCalibur, Becton Dickinson, Franklin Lakes, NJ). Excitation was at 488 nm and emission was at ~600 nm.

Quantitative mRNA Analysis of UCH Isozyme Genes by Real-Time PCR

SYBR Green-based real-time quantitative RT-PCR (ABI PRISM 7700 Sequence detection system, Columbia, MD) was performed [33, 35] in SYBR Green Master mix using the following primers; UCH-L1, 5′-TTCTGTTCAACAACGTGGACG-3′ and 5′-TCACTGGAAAGGGCAT TCG-3′; UCH-L3, 5′-TGAAGGTCAGACTGAGGCACC-3′ and 5′-AA TTGGAAATGGTTTCCGTCC-3′; UCH-L4, 5′-AAACAAACCATCAG CAATGCC-3′ and 5′-GACCCTGATTCAAAGTGCACC-3′; UCH-L5, 5′-TTTTCTTTTCAAGTGGCAGCC-3′ and 5′-GATAGCCTGAGTGGC ACAAGC-3′; and β-actin, 5′-CGTGCGTGACATCAAAGAGAA-3′ and 5′-CAATAGTGATGACCTGGCCGT-3′. For comparing relative UCH isozyme gene expression in isolated germ cells and Sertoli cells, the formula 2^{-ddCt} was used to calculate relative expression levels compared with spermatogonia of two-week-old mice. For comparing the expression level of UCH isozyme genes in the time course of testicular maturation, the formula 2^{-ddCt} was used to calculate relative expression levels compared with the testes of 5-day-old mice.

Western Blotting of UCH-L1 and UCH-L3 from Isolated Cells

Total protein was extracted [24] from isolated testicular cells or whole testes of 5-, 7-, 15-, 19-, 21-, 23-, 26-, and 33-day-old Balb/c mice. Control extracts were obtained from testes of *gad* and *Uchl3* knockout mice. For preparation of antibodies, we designed two specific peptides, AQHEN-FRKKQIEELKGQEVSPK (R891A, GenBank no. NP_057932, residues 57–78) and EKYEVFRTEEEEKIKSQGQDVTSS (R837A, GenBank no. NP_035800, residues 60–83) corresponding to mouse UCH-L1 and UCH-L3, respectively. Polyclonal antibodies against R891A and R837A were raised in rabbits and the IgG fraction was isolated (Tana Laboratories, L.C., Houston, TX). Each sample was adjusted to 5 μg protein/10 μl and subjected to SDS-PAGE (15% acrylamide; XV Pantera gel; DRC, Tama, Japan). After transferring the proteins to a nitrocellulose membrane and blocking with 5% skim milk, the membranes were incubated at 4°C overnight with the primary antibody to UCH-L1 (1:1000) or UCH-L3 (1:400). The membranes were then incubated with peroxidase-conjugated goat anti-rabbit IgG (H+L) (1:10 000; Pierce, Rockford, IL) for 60 min at room temperature. Immunoreactivity was visualized using the SuperSignal detection kit (Pierce) and analyzed with a ChemiImager (Alpha Innotech, San Leandro, CA).

Immunohistochemistry of UCH-L1 and UCH-L3

Tissues were fixed in vivo with 4% paraformaldehyde in phosphate-buffered saline (PBS) and embedded in paraffin, and sections (4 μm thickness) were treated with absolute methanol containing 3% H_2O_2 for 30 min to block endogenous peroxidase activity. After blocking with 10% goat serum for 1 h at room temperature, the sections were incubated at 4°C overnight with antibodies to UCH-L1 (1:500) or UCH-L3 (1:200) diluted in PBS containing 1% BSA. The sections were then incubated with fluorescein isothiocyanate-conjugated anti-rabbit IgG (1:200, Jackson ImmunoResearch, West Grove, PA) for 1 h at room temperature and examined by confocal laser scanning microscopy (Olympus, Tokyo, Japan).

RESULTS

Isolation of Spermatogenic Cells and Sertoli Cells

Using the c-kit antibody, we isolated an average of 17 × 10^5 type A spermatogonia from ten 2-wk-old juvenile mice and an average of 3.5 × 10^5 type A spermatogonia